\$ S ELSEVIER

Contents lists available at ScienceDirect

Field Crops Research

journal homepage: www.elsevier.com/locate/fcr



Planet's Biomass Proxy for monitoring aboveground agricultural biomass and estimating crop yield

Pierre C. Guillevic ^{a,*}, Benjamin Aouizerats ^a, Rogier Burger ^a, Nadja Den Besten ^a, Daniel Jackson ^a, Margot Ridderikhoff ^a, Ariel Zajdband ^b, Rasmus Houborg ^b, Trenton E. Franz ^c, G. Philip Robertson ^d, Richard De Jeu ^a

- ^a Planet Labs PBC, Haarlem 2011 VK, the Netherlands
- ^b Planet Labs PBC, San Francisco, CA 94107, USA
- ^c School of Natural Resources, University of Nebraska-Lincoln, Lincoln, NE 68583, USA
- d Dept. of Plant, Soil and Microbial Sciences, Kellogg Biological Station, Michigan State University, Hickory Corners, MI 49060, USA

ARTICLE INFO

Keywords: Remote sensing Planet's Biomass Proxy Crop growth monitoring Field data Crop biomass Crop yield

ABSTRACT

In the context of increasing environmental change, monitoring crop conditions throughout the growing season is critical for agricultural management, risk mitigation and early assessment of food, feed, fuel and fiber production. Satellite Earth observations can provide frequent and spatially continuous measures of cropping systems to support informed agricultural decisions. However, current analysis-ready satellite data are based on optical observational systems that do not provide land surface information under cloudy conditions, and therefore cannot ensure a continuous and operational monitoring of dynamic systems such as crops. To fill this gap, Planet developed the Biomass Proxy product which provides a timely and analysis-ready relative measure of the above-ground crop biomass daily at 10 m spatial resolution. Based on Earth observations from Sentinel-1 and Sentinel-2 constellations, the Biomass Proxy is a cloud-free vegetation monitoring product for agricultural management at scales varying from the intra-field to the national scale.

The objective of this study was to quantify the sensitivity of Planet's Biomass Proxy to crop biomass dynamics and yield. Field data representative of various agricultural systems and climates from the University of Nebraska-Lincoln and Michigan State University were used to characterize the relationships between the Biomass Proxy and the biomass of corn, winter wheat and soybean fields. Results demonstrated the sensitivity of the Biomass Proxy to changes in crop fresh biomass throughout the growing season, and the potential of the product to detect rapid changes in plant growth due to agricultural practices or environmental stresses, such as nitrogen or water deficiencies. The Biomass Proxy was highly correlated with the plant fresh biomass ($R^2 > 0.9$ for corn) allowing for near real-time monitoring of crop growth and management decisions such as irrigation water, fertilizer and fungicide applications depending on the crop. Using regressions, the Biomass Proxy was able to explain 80 % of the yield variance of agricultural fields one to two months before harvest, allowing marketing and logistic decisions to be made with a better knowledge of the crop status.

The Biomass Proxy is a unique satellite-based product used to characterize the various components of agricultural ecosystems, early detect crop growth anomalies, or assess crop yield. The Biomass Proxy provides real time information on crop conditions and environmental threats, helping mitigate risks by supporting agricultural decisions.

1. Introduction

Due to agricultural intensification and a changing and very variable climate, the fundamental environmental challenge for agriculture is to optimize the use of existing resources and ensure efficient and sustainable agricultural practices and water management (FAO, 2022). Although monitoring crop and pasture conditions is highly relevant for agricultural management, risk mitigation and commodity market transparency (Becker-Reshef et al., 2019), accurate assessment of shortfalls in agricultural production early in the season is still

^{*} Correspondence to: Planet Labs PBC, Wilhelminastraat 43a, Haarlem 2011 VK, the Netherlands. *E-mail address*: pierre@planet.com (P.C. Guillevic).

challenging at scales varying from the individual field to the agricultural region (Hatfield et al., 2020). Yield forecasts early in the season are mainly based on field surveys, empirical relationships using weather or remote sensing inputs, or crop modeling. Through labor-intensive and time-consuming processes, cereal crop yield can be reliably predicted using in situ observations such as the numbers of stems per unit of area and grains per head (Slafer et al., 2023). Over large areas, where field data are sparse or usually not available, satellite observations can provide frequent and spatially continuous measure of agricultural systems. The increasing availability of satellite-derived analysis ready data facilitates informed decision making to optimize management and production (Whitcraft et al., 2015a), and contributes to mitigate the impact of agriculture on environmental resources and climate variability through more efficient use of agricultural inputs (Basso and Liu, 2019; Hatfield et al., 2020). In previous research, Earth observations in various electromagnetic spectral domains, i.e. visible, infrared and microwave, have already been used to obtain relevant and timely information to support early detection of crop anomalies due to pest, crop diseases or environmental stresses (Funk and Budde, 2009; Gao et al., 2018; Hatfield et al., 2020; Laluet et al., 2023), or to constrain crop models (Basso and Liu, 2019; Lievens et al., 2017) with the objective to optimize field operations that usually translates into better environmental outcomes, such as reducing fertilizer losses or freshwater irrigation (El Hajj et al., 2023; Laluet et al., 2023).

Satellite remote sensing in the shortwave spectral domain has been used for crop monitoring and crop parameter retrieval since the 80's (MacDonald and Hall, 1980; Tucker, 1979; Tucker et al., 1985). Numerous previous studies have focused on the use of vegetation indices based on multispectral data to estimate crop growth and yield (Franch et al., 2021; Franz et al., 2020; Liu et al., 2010; Montero et al., 2023; Zhang and Zhang, 2016). At national scales, operational warning systems have been developed based on the use of the Normalized Difference Vegetation Index (NDVI) derived from the Advanced Very High-Resolution Radiometer (AVHRR), the Moderate Resolution Imaging Spectroradiometer (MODIS) or Sentinel-3 to estimate crop growth status or forecast yield for agricultural monitoring and food security with a spatial resolution of 1-5 kilometers. Examples of such products are: the Group on Earth Observation's Global Agricultural Monitoring (GEOGLAM) system (Becker-Reshef et al., 2019, 2010), the UN Food and Agriculture Organization (FAO) Global Information and Early Warning System (GIEWS) (Rashid, 2003) and the European commission's Joint Research Centre (JRC) Monitoring Agricultural ResourceS (MARS) (Van Der Velde et al., 2019).

Agricultural systems are very dynamic with significant temporal changes in aboveground biomass due to environmental or management events, such as grazing, water shortage and irrigation, pest and diseases or fertilization. However, satellite observations in the optical domain do not provide information about the land surface under cloudy conditions and therefore cannot ensure continuous agricultural monitoring (Whitcraft et al., 2015b). Using ground station measurements and MODIS cloud masks, Lagouarde et al. (2013) estimated that a one-day revisit polar-orbiter system could provide on average one cloud-free image every five days over Europe. Over areas with frequent and persistent cloud coverage, the computation of average or cumulative observations used to assess crop yield can be significantly impacted by the availability of clear-sky observations (Gao et al., 2018) and alternative products based on microwave observations should be considered.

Spaceborne Synthetic Aperture Radar (SAR) systems at frequencies varying from 1 to 12 GHz for vegetation applications, provide timely and reliable backscattered surface information regardless of the presence of clouds and sun illumination. In addition to the characteristics of the radar system, i.e., frequency, polarization, and viewing configurations, SAR data depend on dielectric and geometric properties of the individual components of the land surface and their distribution within the canopy (Ulaby and Wilson, 1985; Ulaby et al., 1981; Vermunt et al., 2022). Crop canopy characteristics may rapidly vary through the

growing season depending on crop development, environmental conditions and stresses. SAR can then be used to monitor soil and vegetation water dynamics and derive surface biophysical parameters, such as soil moisture, vegetation optical depth, vegetation water content or biomass information (Attema and Ulaby, 1978; Ulaby et al., 1981). Prior studies have already demonstrated the potential of radar observations in C-band (around 5 GHz) and higher frequencies to assess crop dynamics and production (see reviews by Liu et al., 2019, McNairn and Brisco, 2004 and Steele-Dunne et al., 2017). Therefore, multi-frequencies, multi-temporal and/or multi-polarimetric SAR data are commonly used to perform crop classification (Bouvet et al., 2014; Chen and Mcnairn, 2006; d'Andrimont et al., 2021; Deschamps et al., 2012; Le Toan et al., 1997; McNairn et al., 2014; Skriver et al., 2011), monitor and identify key phenological stages (McNairn et al., 2018; Mercier et al., 2020; Qadir et al., 2023; Veloso et al., 2017) or derive crop biophysical parameters, such as leaf area index (LAI) (Fieuzal and Baup, 2017; Jiao et al., 2011; Liu et al., 2015; Maity et al., 2004; McNairn et al., 2012; Prevot et al., 1993a; Tao et al., 2016; Ulaby et al., 1984), vegetation optical depth (El Hajj et al., 2019; Vreugdenhil et al., 2020), plant water content (Liu et al., 2015; Prevot et al., 1993b; Vreugdenhil et al., 2018) or crop biomass (Fieuzal and Baup, 2017; Wiseman et al., 2014). A summary of the main parameter retrieval studies and key findings is

The reported methods in Table 1 are based on various polarimetric information and indices to derive biophysical parameters of the main cultivated crops (i.e., corn, wheat, soybean and rice) using regression analysis, machine learning approaches or process-based models. Using the water cloud model, a simplified physically based model adapted to derive soil or vegetation parameters from remote sensing, Attema and Ulaby (1978) and Ulaby et al. (1984) showed good correlations between radar backscattering coefficients and LAI for corn, wheat and sorghum. Compared to the optical domain, only a few studies have focused on using SAR data to assess crop yield early in the season. Using an artificial neural network to assess wheat yield, Fieuzal and Baup (2017) have found better performance of the system when using polarimetric SAR data rather than optical or single polarization SAR data. Due to the strong correlation between vegetation water content and fresh biomass, radar backscatter coefficients were also used to monitor the diurnal pattern of water in plants during active growth, manage water resources and detect vegetation water stresses (Brisco et al., 1990; Steele-Dunne et al., 2012).

However, despite a substantial body of research based on SAR imagery, up until recently no SAR-based analysis-ready product has been made available for near real time crop monitoring at the global scale. As previously mentioned, current global assessments of crop conditions are only based on optical data at moderate spatial resolution (km scale), which are not appropriate over regions with high cloud coverage and/or small-scale food producers (<5 ha).

In May 2023, Planet launched the Biomass Proxy product, which provides a unique, timely and analysis-ready relative measure of aboveground crop biomass on a daily basis, with a spatial resolution of 10 m. The Biomass Proxy uses a combination of Earth observations from Sentinel-1 and Sentinel-2 constellations to perform a cloud-free vegetation monitoring at scales varying from the intra-field scale to the national scale (Burger et al., 2024). As part of Planet's Planetary Variables solutions that also include Soil Water Content, Land Surface Temperature, Forests Carbon and Field Boundaries products, the Biomass Proxy was designed to facilitate near real time agricultural monitoring to assist governments, non-governmental organizations, research institutions and food producers to perform informed decisions related to agricultural management and production forecast, sustainable agriculture, and crop insurance. Across agricultural fields, spatiotemporal variations in the Biomass Proxy help characterize the different components of agricultural ecosystems, early detect crop growth anomalies, optimize agricultural practices and agrochemical input efficiency, or schedule field activities such as crop harvesting, grass mowing and grazing practices.

Table 1
Summary of previous studies using radar Earth observations to monitor vegetation dynamics and/or assess crop yield. Relevant specifications and key findings are also summarized.

Reference	Satellite data	Crop types/location	Relevant particularities	Key findings
El Hajj et al. (2019)	Sentinel-1, Sentinel-2	Barley, fallow, oat, and wheat in Catalonia, Spain	Better ability of VV than NDVI to identify plant water loss periods	High correlations between VV polarization and VOD (\mathbb{R}^2 varying from 0.39 and 0.61)
Fieuzal and Baup (2017)	TerraSAR-X, Radarsat-2 and Spot 4-5	Wheat near Toulouse, France	Neural network combined with optical and radar data	High correlations ($R^2 = 0.76$) between yield and combination of VV and HH in C-band
Gorrab et al. (2021)	Sentinel-1	Wheat near Toulouse, France	VV, VH, VV/VH, VV*VH cumulated or not over various growth periods	High correlations (R ² >0.9) between cumulative VV*VH and plant height and total dry biomass
Jiao et al. (2011)	RADARSAT – 2 polarimetry	Corn and soybean	LAI values from optical data	High correlations (R ² >0.9 for corn and R ² >0.7 for soybean) between all polarimetric parameters and biomass
Kim et al. (2012)	L, C and X-bands field polarimetric scatterometer	Rice and soybean in South Korea	Radar vegetation Index	High correlations between L and C-band (R ² =0.94) RVI and VWC
Mattia et al. (2003)	C-band field scatterometer	Wheat near Matera, Italy	Incidence angles from 20 to 60°	High correlations (R^2 =0.94) between HH/VV at 40° and fresh biomass
McNairn et al. (2012)	RADARSAT-2 polarimetry	Wheat, oat and barley fields in western Canada during AgriSAR	co and cross polarization coefficients, various cross ratios and polarimetric decompositions	HV coefficient and entropy were highly correlated to LAI ($R^2 > 0.8$) for wheat and oat.
Ouaadi et al. (2020)	Sentinel-1	Wheat near Marrakech, Morocco	co and cross polarization coefficients, cross ratio, coherence	Good correlations between VV and the above ground dry biomass (R ² >0.6)
Prevot et al. (1993a, 1993b)	ERASME airborne scatterometer	Wheat, Orgeval basin, France	X and C bands, multi-incidence, inversion of the water cloud model	Good correlations with VWC (R ² >0.5)
Prevot et al. (1993–2)	Ground-based dual- frequency scatterometer RAMSES	Wheat, Orgeval basin, France	X and C bands, inversion of the water cloud model	Good correlations with LAI (RMSE of 0.64 $\ensuremath{\text{m}}^2$ $\ensuremath{\text{m}}^{-2}$)
Veloso et al. (2017)	Sentinel 1	Winter cereals, rapeseed, corn, soybean and sunflower, southwestern, France	Detailed description of VV, VH and VV/VH time series	High correlations between VV/VH and NDVI (R ² of 0.91, 0.74, 0.3, 0.82, 0.08 for corn, cereals, rapeseed, soybean and sunflower)
Vreugdenhil et al. (2018)	Sentinel 1	Rapeseed, cereal and corn in Petzenkirchen, Austria	Cross-polarized ratio CR (VH/VV)	High correlations between CR and VWC for corn and cereals (R ² of 0.87 and 0.63, resp.). Lower correlations for rapeseed.
Wiseman et al. (2014)	RADARSAT-2 polarimetry	Canola, corn, soybean, and spring wheat fields in western Canada	Dry biomass of leaves and stems for corn	High correlations (R ² >0.7) between most of polarimetric parameters and corn biomass components

The Biomass Proxy provides early warning on crop conditions and environmental threats, helping mitigate risk by supporting agricultural decisions.

The key objective of this paper is to quantify the sensitivity of Planet's Biomass Proxy product to crop biomass dynamics and crop yield using field validation datasets collected by the Eastern Nebraska Research Education and Extension Center (ENREEC) of the University of Nebraska-Lincoln and the Kellogg Biological Station experiment at Michigan State University from 2019 to 2022. The field validation datasets include aboveground biomass measurements of the three major crops grown in the USA, i.e., corn, winter wheat and soybean. Like NDVI, the Biomass Proxy is a relative indicator/index that cannot be directly validated using ground-based references. To overcome this difficulty, the following hypotheses were used to evaluate the product's ability to characterize agricultural systems: (1) based on radar signals in C-band, the Biomass Proxy accurately describes time series of crop fresh biomass and accounts for the impact of environmental stresses through the growing season, and (2) the amount of aboveground fresh biomass is a good indicator of crop yield for the selected crops. After a brief description of the satellite data, the processing algorithm and the field experiments in the first section, we will demonstrate and quantify the ability of Biomass Proxy to monitor plant fresh biomass of irrigated and rainfed corn and soybean fields in Nebraska, and to forecast yield amount and variability early in the growing season of crop systems associated with a wide range of agricultural practices including conventional and organic certified treatments, regenerative agriculture and biodiversity, no-tillage and crop rotation. In the last section, results and the validity of our hypotheses will be discussed.

2. Materials and Methods

This section describes Planet's Biomass Proxy product, the field validation datasets and the methodology used to compare the Biomass

Proxy to in situ measurements.

2.1. Planet's Biomass Proxy

The Biomass Proxy algorithm (Burger et al., 2024) represents a spatio-temporal fusion of radar and optical data from Sentinel 1 and Sentinel 2 constellations part of the European Commission's Copernicus Earth Observation program.

2.1.1. Sentinel-1 data and the radar cross ratio

Until 2021, the Sentinel-1 mission (Torres et al., 2012) consisted of two polar-orbiting satellites, Sentinel-1A and Sentinel-1B launched in 2014 and 2016, respectively. Due to an anomaly related to the electronics power supply, the Sentinel-1B mission ended in December 2021. Sentinel-1 satellites carry a SAR system in C-band (5.405 GHz). We use the Interferometric Wide swath (IW) and Ground Range Detected (GRD) imagery mode providing dual-polarization imagery, i.e., backscatter coefficients in Vertically emitted-Vertical received (VV) and Vertically emitted-Horizontally received (VH) polarizations, with a spatial resolution of 10 m over a swath of 250 kilometers. The revisit time period of a single Sentinel-1 satellite is 12 days, and temporal coverage is between 1 and 4 days over Europe, and 6 days over the United States when using both Sentinel-1A and Sentinel-1B. The continuity of the Sentinel series is guaranteed for the next decades by the Copernicus program allowing operational long-term agricultural monitoring capabilities. In addition, the launch of Sentinel 1-C is currently scheduled for the end of 2024. Regarding our experimental sites, the acquisition plan of Sentinel 1-B did not include part of Nebraska in the United States. The revisit time period of Sentinel-1 was 12 days at Mead, Nebraska and was 6 days before December 2021 and 12 days after December 1st, 2021 at Kellogg Biological Station, Michigan.

The radar signature of vegetated surfaces consists of three main components describing direct backscatter from the vegetation canopy,

backscatter from the soil attenuated by the canopy and multiple scattering effects due to interactions between the vegetation and soil (Attema and Ulaby, 1978; Steele-Dunne et al., 2017; Ulaby et al., 1981). Therefore, the vegetation signal must be isolated to effectively use Sentinel-1 to monitor agricultural systems. As a first approximation, backscatter coefficients in VH polarization are more sensitive to volume scattering and the presence of vegetation, while backscatter coefficients in VV polarization are more responsive to changes in surface scattering (Attema and Ulaby, 1978; Ulaby et al., 1981; Veloso et al., 2017). Therefore, ratios of co-polarized and cross-polarized backscatter observations, such as the Radar Vegetation Index (Kim and van Zyl, 2009) and the Cross Ratio (Paloscia et al., 1999; Veloso et al., 2017; Vreugdenhil et al., 2018), were commonly used to monitor crop growth and conditions. Moreover, previous studies showed that the ratio of Sentinel 1 backscatter coefficients in VH and VV polarizations (VH/VV) significantly reduced the effects of soil moisture, incidence angle, and soil-vegetation interaction effects (Harfenmeister et al., 2019; Veloso et al., 2017) enhancing the vegetation contribution to radar measurements. The cross ratio VH/VV is used in the Biomass Proxy algorithm. It should be noted that rough soils, water logging and intercepted water by the canopy may also cause depolarization of radar signatures and may significantly affect cross-polarized backscatter coefficients (den Besten et al., 2023; Vermunt et al., 2022; Vreugdenhil et al., 2020), which explains the non-zero values of the Biomass Proxy we observed for bare soils. However, excluding early growth stages and senescence, the contribution of vegetation canopy in the radar signal is predominant (Mattia et al., 2003) and contributes up to 90 % on average when the crop LAI is higher than 3 (Wiseman et al., 2014).

2.1.2. Sentinel-2 and the NDVI

The Sentinel-2 mission (Gascon et al., 2017) consists of two polar-orbiter satellites, Sentinel-2A and Sentinel-2B launched in 2015 and 2017, respectively. The Sentinel-2 Multi-Spectral Instrument (MSI) provides surface reflectance products in 13 spectral bands in the visible, near infrared and shortwave infrared range of the electromagnetic spectrum. The combined Sentinel-2A and Sentinel-2B platforms ensure a revisit period of five days. The spatial resolution varies from 10 to 60 m depending on the acquisition mode or the spectral domain. To enhance vegetation signals, NDVI products based on surface reflectances in the red (band 4 centered at 665 nm) and near infrared (band 8 centered at

842 nm) domains at 10 m spatial resolution are used in the Biomass Proxy algorithm (Burger et al., 2024).

2.1.3. Biomass Proxy retrieval algorithm

A full description of the Biomass Proxy algorithm is provided by Burger et al. (2024). The main steps of the algorithm are summarized below and illustrated in Fig. 1:

- Input imageries pre-processing, NDVI and radar cross ratio time series generation. This first step primarily represents preprocessing of the optical imagery using multiple cloud masking routines, i.e., Fmask (Zhu et al., 2015), S2cloudless (Sanchez et al., 2020) and Sen2Cor (Baetens et al., 2019), and the application of multi-temporal and spatial filtering to reduce speckle effects in radar images (Lee, 1983).
- 2. Scaling the radar Cross Ratio (CR) to the NDVI domain of variation. Based on a large set of fields randomly selected all around the world, regression analysis between CR, i.e., the ratio of backscatter coefficients in VH and VV polarizations (VH/VV), and NDVI data was used to scale the CR signals to the NDVI variation range, which is needed for the data fusion step.
- 3. Generate a field averaged Biomass Proxy. For each field, the scaled radar cross ratio and the NDVI are combined using static and dynamic weighing strategies driven by the uncertainties and the relative recency of the optical and radar images to derive a fused vegetation signal on a daily basis.
- 4. Downscaling from field average to 10 m spatial resolution. A dynamic weighting strategy is applied in the spatial domain to disaggregate the field averaged Biomass proxy to a 10 m resolution image using the relative spatial distribution of the radar CR and the NDVI.

2.2. Field validation datasets

Ground-based measurements of crop biomass and/or yield collected at two different experimental sites from 2019 to 2022 were used to evaluate the ability of the Biomass Proxy to inform on crop biophysical parameters (Fig. 2).

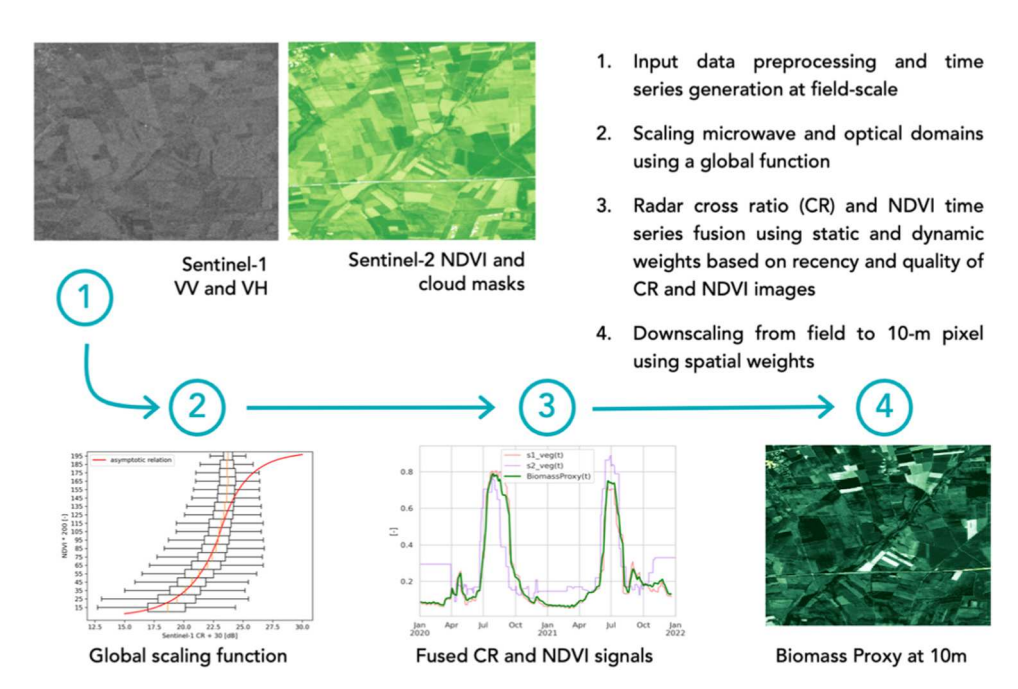


Fig. 1. Schematic representation of the Biomass Proxy algorithm. The different relations used to define the scaling function are described by Burger et al. (2024).



Fig. 2. Representation of the experimental design of the three experimental fields near Mead, Nebraska (left) and the Main Cropping System Experiment (MCSE) of the Kellogg Biological Station in Michigan (right). In Nebraska, the Intensive Measurement Zones (IMZ, red circles) represent the sampling locations where plants were collected for biomass measurements. In Michigan, for each crop, four different treatments (letter T) are evaluated at the Kellogg Biological Station. Each treatment is applied to six different replicated fields (letter R).

2.2.1. Mead, Nebraska experiment

The long-term field experiment near Mead, Nebraska, USA has been managed by ENREEC, the University of Nebraska-Lincoln since 2001 with the objective to document the carbon exchanges in agroecosystems and develop strategies to mitigate the increase in atmospheric carbon dioxide concentration (Suyker et al., 2005; Verma et al., 2005). It consists of three large production fields of 50–65 ha associated with different cropping systems. Two fields are irrigated with pivot center irrigation systems and represent continuous corn (*Zea mays*) (field #1 in Fig. 2) and a corn-soybean (*Glycine max L.*) rotation (field #2) system, respectively. The third field is under a rainfed corn-soybean rotation system (field #3). In these fields, no tillage was applied. The sites are part of the Ameriflux network (Baldocchi et al., 2001) collecting meteorological and land surface flux data.

In this paper, ground datasets describing the crop biomass components, i.e., fresh and dry biomass of the stems, the leaves and the reproductive parts of the plants (Fig. 3), were used. Fresh and dry matter are determined by destructive sampling and weighting before and after oven drying of the crop samples. Crop yield is derived from dry matter measurements of the reproductive part of the plant expressed per unit area. Fresh biomass is made up of organic matter and water, and the percentage of moisture remaining in the dry matter is around 15 % for corn and 13 % for wheat. The biomass samples were collected at six different Intensive Measurement Zones (IMZ) within each field (Fig. 2) describing the within field spatial variability of soil characteristics affecting crop conditions (Verma et al., 2005). Each IMZ is a 30 by 30-meter area designated for scientific observations. It is a clearly marked area in the field such that farm managers are aware of the measurements and instruments and can plan field operations accordingly. Destructive samples are collected at the main crop physiological stages (every 5-15 days) throughout the growing season. Five to seven entire corn plants and fifteen to thirty entire soybean plants are removed from each IMZ for laboratory measurements of biomass. For corn, the different plant samples have been individually measured and recorded in the database, and the replicates can be used to assess field

measurement uncertainties. For soybean, individual plant data is not available, and each recorded IMZ data represents a bulk measurement including all the plants.

2.2.2. LTER Kellogg Biological Station

The Main Cropping System Experiment (MCSE) of the Kellogg Biological Station (KBS) was initiated in 1988 near Hickory Corners, Michigan to assess ecosystem services provided by ecological farming (Philip Robertson et al., 2014; Robertson and Hamilton, 2015). The experiment is part of the US Long Term Ecological Research (LTER) Network (Robertson and Hamilton, 2015). The annual cropping systems are corn, soybean and winter wheat (Triticum aestivum), with the rotations managed in four different treatments. The first treatment represents conventional cropping practices used in Michigan, including tillage and genetically engineered soybeans and corn. The second treatment is similar to the first one but without tillage applied. The third treatment, a reduced-input system, is like the conventional system but with about one third of the chemical inputs and winter cover crops to provide additional nitrogen. The fourth treatment is managed biologically, with no synthetic chemical inputs or manure but with cover crops. Twenty-four fields are considered in this study representing six different replicates of each treatment (Fig. 2). Yield data for each experimental field was based on combine harvester measurements of the entire crop area and corrected to a standardized moisture level of 15.5 % for corn and 13 % for wheat and soybean. The different treatments lead to large variability in crop yield, which represents a valuable dataset for evaluating the Biomass Proxy and its crop scouting capabilities.

2.3. Relations between the Biomass Proxy, crop biomass and yield

Comparisons between the Biomass Proxy and field measurements require matchup datasets with consistent spatial and temporal representativeness. Depending on the experimental design, the spatial representativeness of ground-based biomass and yield measurements is approximatively the IMZ area (i.e., $30\times30~\text{m}^2$) in Nebraska and the

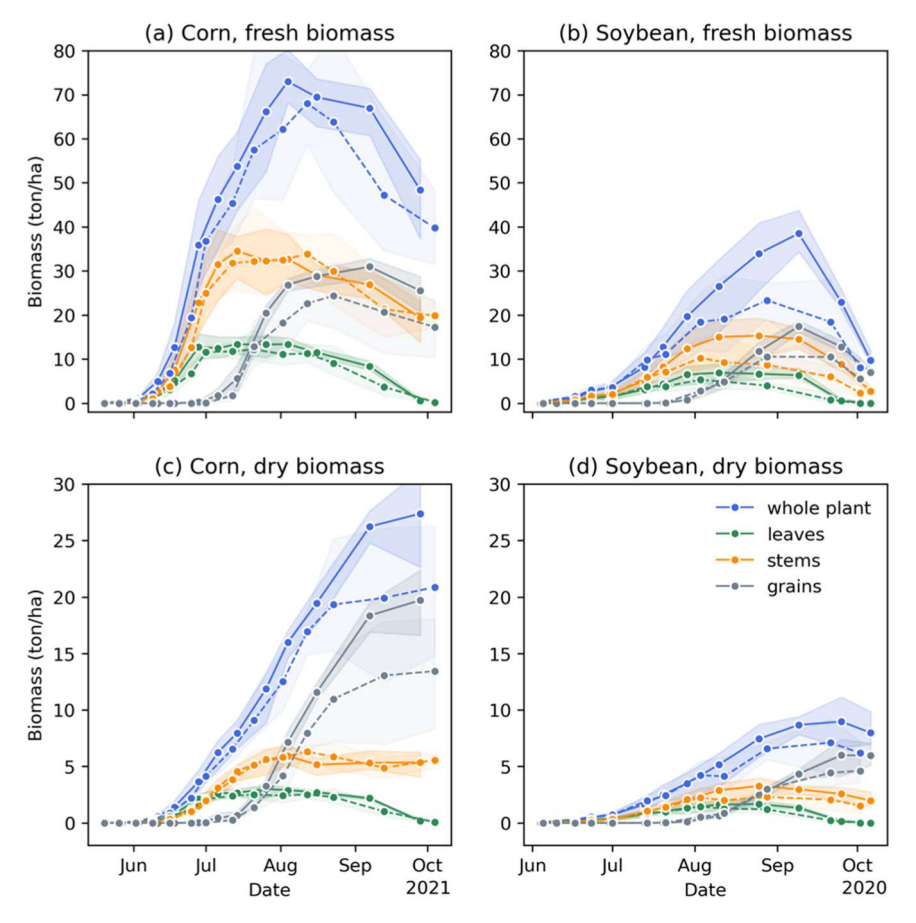


Fig. 3. Fresh (a and b) and dry (c and d) biomass components of corn (a and c) and soybean (b and d) fields at Mead, Nebraska. Data from irrigated (site #2, Fig. 2) and rainfed (site #3, Fig. 2) fields are represented by solid and dashed lines, respectively. Each point represents the average value of biomass components collected at six different IMZ locations per field (see Fig. 2) and the faded envelopes represent the observed minimum and maximum values.

treatment plot area (i.e., 1 ha) in Michigan. Therefore, the Biomass Proxy at 10 m spatial resolution was aggregated over 3×3 and 10×10 -pixel areas covering the IMZ and treatment plots, respectively. The relationships between satellite-derived Biomass Proxy and the different crop biomass components from the field measurements, i.e., whole plant, or fresh and dry biomass of the stems, ears and leaves when available, were characterized by regressions analysis. The strength of each relationship and performance of the regression model was quantified by the coefficient of determination R^2 (Eq. (1)) that represents the proportion of the variation in crop biomass that can be explained by the Biomass Proxy, the Mean Absolute Error (MAE, Eq. (2)) that describes the uncertainty associated with a regression model, and the relative MAE (rMAE, Eq. (3)), respectively. We also used the Standard Error (SE, Eq. (4)) of the mean to assess the likely accuracy of the IMZ-mean biomass estimates based on sample sizes.

$$R^{2} = 1 - \frac{\sum_{i} (y_{i} - \hat{y}_{i})^{2}}{\sum_{i} (y_{i} - \bar{y})^{2}}$$
(1)

$$MAE = \frac{1}{n} \sum_{i=1}^{n} |y_i - \widehat{y}_i|$$
 (2)

$$rMAE = \frac{MAE}{\overline{V}} \times 100\% \tag{3}$$

$$SE = \frac{\sigma}{\sqrt{n}} \text{ with } \sigma = \sqrt{\frac{\sum_{i} (y_i - \widehat{y}_i)^2}{n - 1}}$$
 (4)

With \bar{y} the average value and \hat{y}_i the predicted values of a series of n ground-based biomass measurements y_i . σ is the standard deviation.

Due to Biomass Proxy's sensitivity to vegetation water content and not directly to dry matter, we used different evaluation protocols when comparing the Biomass Proxy with fresh or dry biomass measurements that vary differently through the season (Fig. 3). For fresh biomass, we compared samples collected through the growing season with concurrent biomass proxy values. In the case of dry matter, we compared final crop yield with different indicators characterizing the Biomass Proxy time series through the crop season before harvest: (1) the maximum or peak of Biomass Proxy representing crop maturity, (2) the mean Biomass Proxy over the crop vegetative phase calculated from crop emergence to (1), and (3) the mean Biomass Proxy observed over various Growing Degree Days (GDD) based integration periods (Fig. 4). A GDD-based integration period was defined between two different levels of cumulative GDD (GDD_C) after crop emergence, i.e., starting cumulative GDD and ending cumulative GDD (Fig. 4). For individual or all crop types, the optimal integration period was identified as the one with the highest correlations between the mean Biomass Proxy and crop yield from an ensemble of integration periods defined by cumulative GDD levels varying from crop emergence (0 GDD_C) to harvest (approximatively 1800 GDD_C) with discretization steps of 100 cumulative GDD.

The regression analysis was based on linear and exponential models following Vreugdenhil et al. (2018) and Wiseman et al. (2014). The three crop yield indicators are compatible with operational uses when no information about the type and growth stage of the observed crops are available. Moreover, the cumulative GDD is a valuable indicator to determine consistent integration periods.

In addition, the Biomass Proxy may also depend on the vertical

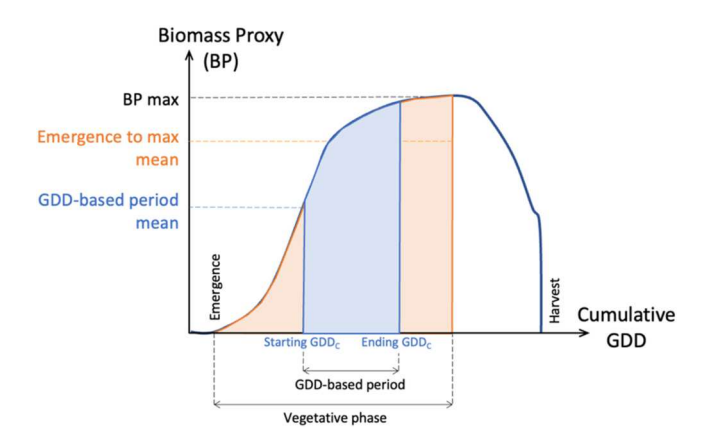


Fig. 4. Representation of the three yield indicators used to characterize the Biomass Proxy time series through the crop season before harvest: (1) the maximum of Biomass Proxy (BP max), (2) the mean Biomass Proxy from crop emergence to (1), and (3) the mean Biomass Proxy over GDD-based integration periods. GDD-based periods were defined between two different levels of cumulative GDD (GDD_C) after emergence: starting GDD_C and ending GDD_C.

(Vermunt et al., 2022) or 3D (Karam et al., 1992) distribution of the vegetation components and water content within the canopy, which are fluctuating in time. As mentioned by Gorrab et al. (2021), the cumulative or average value may be a good indicator of the influence of environmental stresses occurring through the growing season on final yield. The authors showed that cumulative polarimetric indices over vegetative periods were much better descriptors of various winter wheat biophysical parameters than the same indices based on a single satellite overpass (Table 1). In the optical domain, Daughtry et al. (1983) found that a single observation in the crop season had limited value in predicting corn yield, compared to vegetation index values accumulated over the growing season, which could explain around 65 % of the corn yield variance.

2.4. Growing degree days

We used growing degree days (GDD) to assess crop phenological stages and to define the optimal integration periods used to compare mean Biomass Proxy and final crop yield data. GDD are commonly used to estimate crop development rates and phenological stages throughout the growing season. GDD-based models assume that crop development occurs when daily mean air temperature (T_{mean}) is higher than a crop dependent temperature threshold or base temperature (T_{base}) and does not exceed a physiological heat limit characterized by maximum acceptable air temperature (T_{heat}) (Mcmaster, 1997) (Eq. 5).

$$GDD = T_{mean} - T_{base}$$

with
$$GDD = 0$$
 if $T_{mean} < T_{base}$
and $GDD = T_{heat} - T_{base}$ if $T_{mean} > T_{heat}$ (5)

 T_{mean} was calculated for each site location using ERA 5 reanalysis data (Hersbach et al., 2020) from the European Centre for Medium-Range Weather Forecasts (ECMWF) that provide hourly estimates of air temperature at 2-meter height at 0.25 degree resolution. T_{base} and T_{heat} have been respectively set to 10°C and 30°C for corn and soybean, and to 0°C and 25°C for wheat (Mcmaster, 1997).

3. Results

3.1. Analysis of time series of ground-based fresh and dry biomass

We performed a preliminary analysis of the timeseries and the existing relationships between fresh and dry plant matter using ground-based data only. From data collected on fields #2 and #3 characterized

by corn-soybean rotation systems, we observed higher dry biomass production on irrigated (#2) related to rainfed (#3) fields with relative differences in final yield of around 30 % for both corn in 2021 and soybean in 2020 (Fig. 3). Differences in fresh biomass of irrigated and rainfed fields were also observed around the vegetative maturity of the plants but they were more significant for soybean than for corn. An interesting feature was observed for corn where fresh and dry biomass of stems and leaves were quite similar between rainfed and irrigated fields, and differences in grain biomass mainly explained differences in whole plant dry biomass measurements (Fig. 3a and c). This characteristic dynamic was not observed for soybean where observed differences were due to the reproductive parts and the stems. These differences might vary from year to year based on local climate and water stress level. Moreover, fresh and dry biomass variations were not consistent through the entire crop season (Fig. 3). The maximum dry biomass was measured at the end of the season just before harvest and weeks after the peak of fresh biomass that occurred at the end of the vegetative phase. As expected, correlations between fresh and dry crop biomass were much higher when just considering the plant vegetative period rather than the entire crop growing season (Fig. 5). Therefore, and as already stressed by Gorrab et al. (2021), radar data, which are sensitive to crop fresh biomass, may not provide useful information related to the senescence phase of the plant.

We also evaluated the link between fresh biomass and yield and found good correlations between the maximum value of the plant fresh biomass measured during the crop season and the total plant or grain yields, with $\rm R^2$ values around 0.9 and rMAE lower than 13 %, when considering corn and soybean together (Fig. 6). We systematically observed lower correlations between the season's maximum fresh biomass and yield values for irrigated relative to rainfed crops and found poor correlations for irrigated corn fields ($\rm R^2=0.04$). This suggests that the performance of crop yield predictions from space observations sensitive to plant fresh biomass or plant water content, such as the Biomass Proxy, may be reduced in the presence of irrigation that tends to maximize and homogenize the canopy size and density of the different fields.

3.2. Biomass Proxy to monitor crop fresh biomass

Fresh biomass amounts were not collected at KBS, Michigan, and this section is only based on data acquired at Mead, Nebraska. The Biomass Proxy time series and in situ measurements of crop fresh biomass from 2019 to 2022 in Nebraska are represented in Fig. 7. Generally, the Biomass Proxy clearly represents the crop signal but with a few nonvegetation related spikes that are most likely linked to rain events at the beginning of the crop season when the vegetation density is relatively low. The most significant spikes observed early in the 2019 crop season are due to heavy rain events (up to 30 mm per day) in June over young corn plants (LAI lower than 2). The drastic increases in the Biomass Proxy observed during the winter were mainly due to snow events. The occurrence of snow on the ground were verified by visual interpretation of daily PlanetScope observations at 3 m spatial resolution - this point was out of the scope of this paper and was not further discussed. At early growth stages, the Biomass Proxy was highly sensitive to precipitation events as reflected by significant spikes in both 2019 and 2020. As already noted by Mattia et al. (2003), the correlations between the Biomass Proxy and fresh biomass were relatively low early in the season due to a significant contribution of the soil to the radar signal, whereas correlations progressively increased with crop development.

For corn, the Biomass Proxy reached a clear plateau at crop maturity, which may suggest a saturation effect of the C-band radar for high vegetation biomass densities above 55–60 tons per hectare (Fig. 7). The plateau varied slightly from year to year and demonstrated that despite continued crop biomass accumulation, the radar backscatter was less responsive to these growth increments. The Biomass Proxy declined

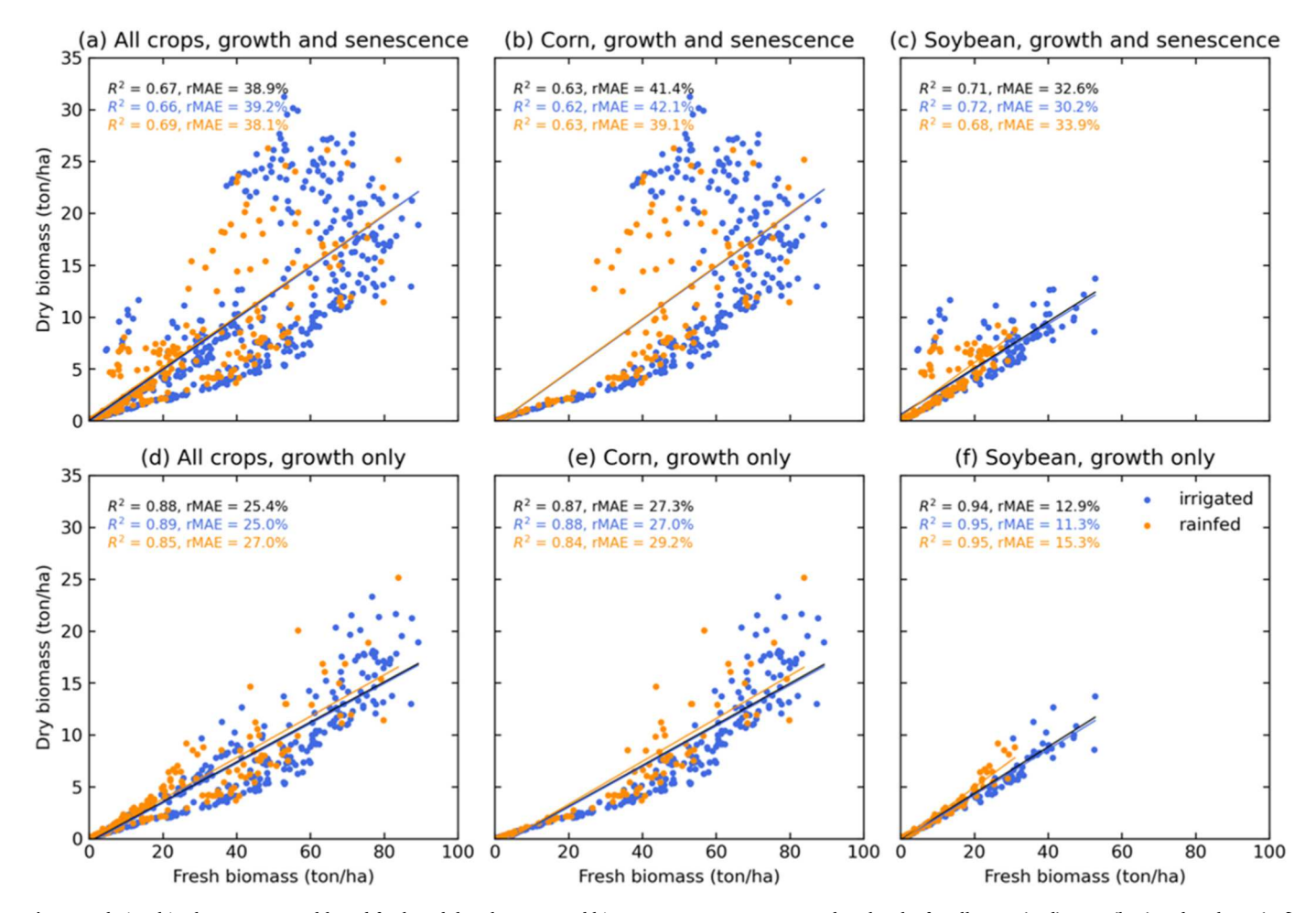


Fig. 5. Relationships between ground-based fresh and dry above ground biomass measurements at Mead, Nebraska for all crops (a, d), corn (b, e) and soybean (c, f) fields accounting for data collected during the growing and senescent periods (a, b, c) and data collected during the growing season only (d, e, f). Correlations coefficients and relative MAE are calculated depending on water management, i.e., irrigated or rainfed fields.

during the senescence period just before harvest except for corn planted in field US-Ne1 in 2020, which was harvested early (end of September) when ears were still green and fresh biomass still at its maximum. Over soybean fields, which have a much lower vegetation density than corn, the Biomass Proxy continuously increased throughout the growing season and the rapid fluctuations observed in the 2020 time series might be explained by a high contribution of wet soil to the radar signal. We did not observe any clear saturation effect for soybean in 2020. Regarding the detection of field management events, the 12-day revisit period of Sentinel-1 over Nebraska explained the delayed response of Biomass Proxy that we observed after harvest, especially in 2021.

We found good agreements between the Biomass Proxy time series and in situ measurements of crop fresh biomass (Fig. 8). For corn, high coefficients of determination were obtained, and the Biomass Proxy was able to explain more than 90 % of the variance of the fresh biomass of the entire plant with a relative MAE of 16 % for irrigated fields and 13 % for rainfed. Corn stems had the largest contribution to the Biomass Proxy signals (R $^2=0.87$) compared to fresh leaves (R $^2=0.67$) or grains (R $^2=0.40$), suggesting that corn stems were the most important plant component in multiple scattering and depolarization effects as already mentioned by Wiseman et al. (2014).

For soybean (Fig. 9), correlation coefficients were still high with R^2 around 0.7 or higher (0.84 for rainfed soybean) when considering the whole plant biomass but lower than those observed for corn. Relative MAE values were significantly higher than for corn, i.e., around 32 % for irrigated fields and 20 % for rainfed. Such differences between corn and soybean might be partly explained by a higher contribution of the

underlying soil to the soybean radar signature. Soybean canopies, which have a lower biomass than corn, attenuate less of the incoming and reflected radiation by the soil. The relative differences between total fresh biomass of irrigated and rainfed fields were higher for soybean (30–45 % at crop maturity depending on the year considered) than for corn (8–23 %) (Figs. 3, 8 and 9). However, such differences had a relatively low influence on the Biomass Proxy. When considering dry matter or yield measurements, measurements depicted lower discrepancies between irrigated and rainfed field production levels.

3.3. Biomass Proxy time series for crop benchmarking

The different treatments at Kellogg Biological Station in Michigan provide a wide range of crop production levels and as such represent a valuable dataset for evaluating the Biomass Proxy and its crop scouting capabilities. Fresh biomass measurements were not available at Kellogg and time series were used to describe the Biomass Proxy signatures associated with the different treatments. The ability of the Biomass Proxy to monitor crops, discriminate and rank field's production are clearly illustrated by the derived time series information (Fig. 10). The time series track the performance of each treatment and identify low levels of biomass that might be due to crop management or environmental conditions. For each crop, we clearly observed a reduced growth and lower accumulation of biomass through the crop season for the biologically certified treatment (T4): the emergence dates were similar, but the crop development phase was much longer than the other treatments (Fig. 10) and associated with lower yield levels (see Section

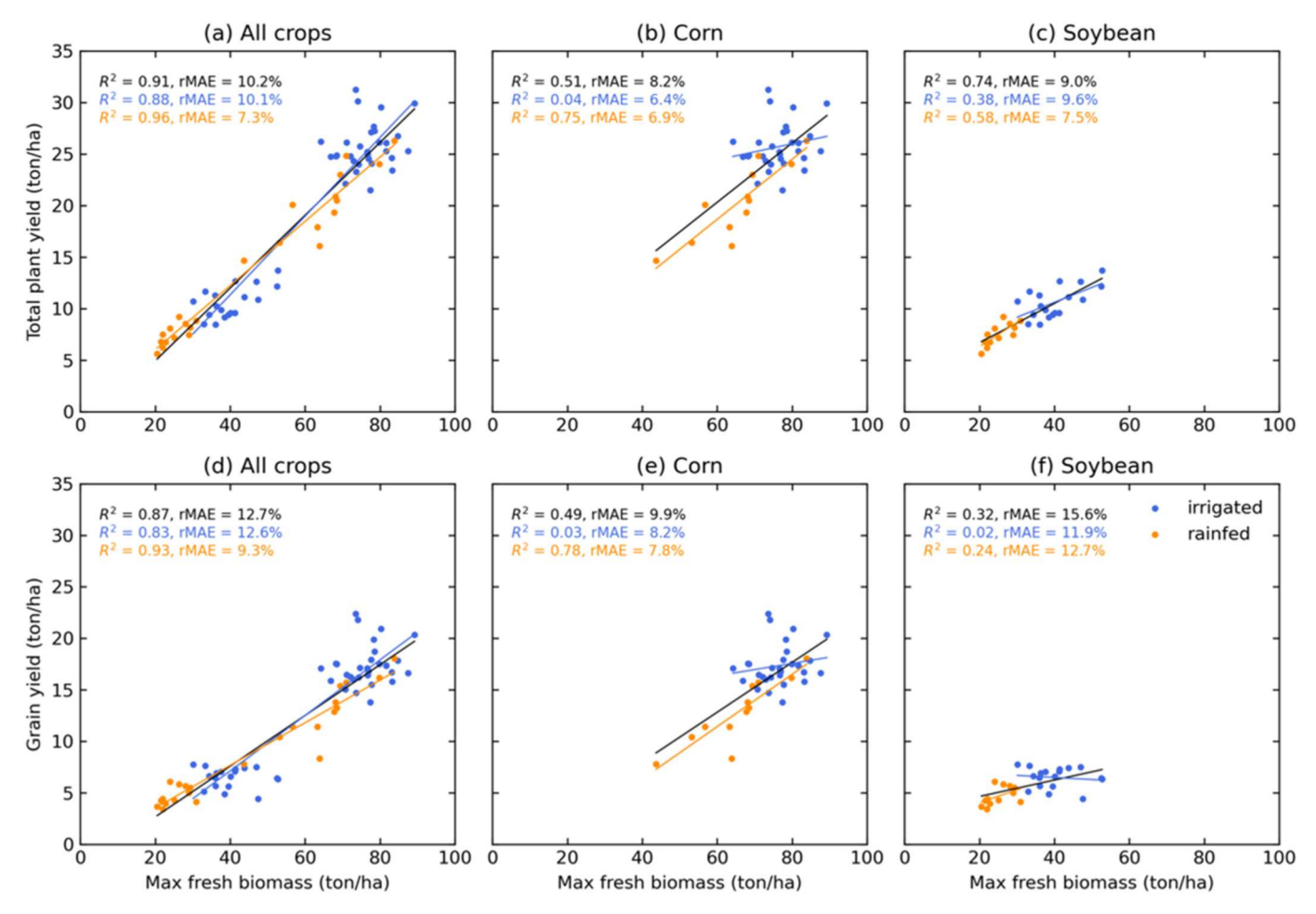


Fig. 6. Relationships between the maximum value of the plant fresh biomass measured during the crop season and the total plant yield (a, b and c) and grain yield (d, e and f), respectively, measured at Mead, Nebraska for all crops (a, d), corn (b, e) and soybean (c, f) fields. Correlations coefficients and relative MAE are calculated depending on water management, i.e., irrigated or rainfed fields.

3.4.2). In general, the T2 treatment representing conventional management with no till, was associated with higher Biomass Proxy values and final yield. The Biomass Proxy time series were also able to detect environmental stresses such as the impact of the 2020 drought on corn production. The temporal signature of corn in 2020 in Michigan did not show a 3-month plateau associated with high biomass values as was observed in Nebraska (Fig. 7). The rapid decrease in corn Biomass Proxy in Michigan after a fast-growing phase in July was associated with very low precipitation in August (50 mm of rain). The final corn yield, around 10 tons per hectare for the T2 treatment, was more than 20 % lower than the T2 yield measured in 2014 that received twice the amount of rain. The Biomass Proxy time series were also able to clearly detect the presence of winter cover crops in 2019 and 2022. For wheat fields in 2019, we observed dips in the Biomass Proxy timeseries. The Biomass Proxy rapidly decreased after the stem elongation and increased again after the heading phase. This effect of phenology and canopy structure was also observed by Mattia et al. (2003) and Vreugdenhil et al. (2018) in the radar cross ratio. Based on a small sample of just a few fields, we noticed that the more pronounced the dip in the Biomass proxy, the higher the crop yield, but further ground observations are required to validate this finding.

3.4. Biomass Proxy to assess crop yield

3.4.1. Sensitivity of the correlations between Biomass Proxy and yield to the integration period

As already mentioned by Gao et al. (2018) for the optical domain and

Gorrab et al. (2021) for the microwave domain, cumulative or average values of vegetation indices are more correlated to crop yield than observations from a single satellite overpass. To verify these results and identify the integration periods that provide the highest correlations between the Biomass Proxy and crop yield, we compared final crop yield with three indicators characterizing the Biomass Proxy time series through the crop season: (1) the maximum of Biomass Proxy, (2) the mean Biomass Proxy value from crop emergence to maximum of Biomass Proxy, and (3) the mean Biomass Proxy observed over various GDD based integration periods (see Fig. 4). To evaluate the third indicator, we first identified the integration periods providing the highest correlations between the mean Biomass Proxy and crop yield from an ensemble of integration periods defined by varying cumulative GDD levels (see Fig. 4). The regression analysis was done for all crops and individual crop types, accounting for all sites (Fig. 11). Results are summarized in Table 2.

When considering all crops together, the optimal GDD-based integration period was obtained between 100 and 1100 cumulative GDD and was associated with a coefficient of determination higher than 0.8 and a relative MAE around 23 % when using an exponential regression model (Fig. 11, Table 2). The integration period represented the vegetative phase only and did not include the senescence phase. When looking at individual crops, the linear regression model was providing better results than the exponential model with coefficients of determination of 0.80, 0.60 and 0.69 for corn, soybean and wheat, respectively, and relative MAE lower than 19 % (Fig. 11, Table 2). When accounting for all crops and sites, the range of yield varied from around 2 tons per

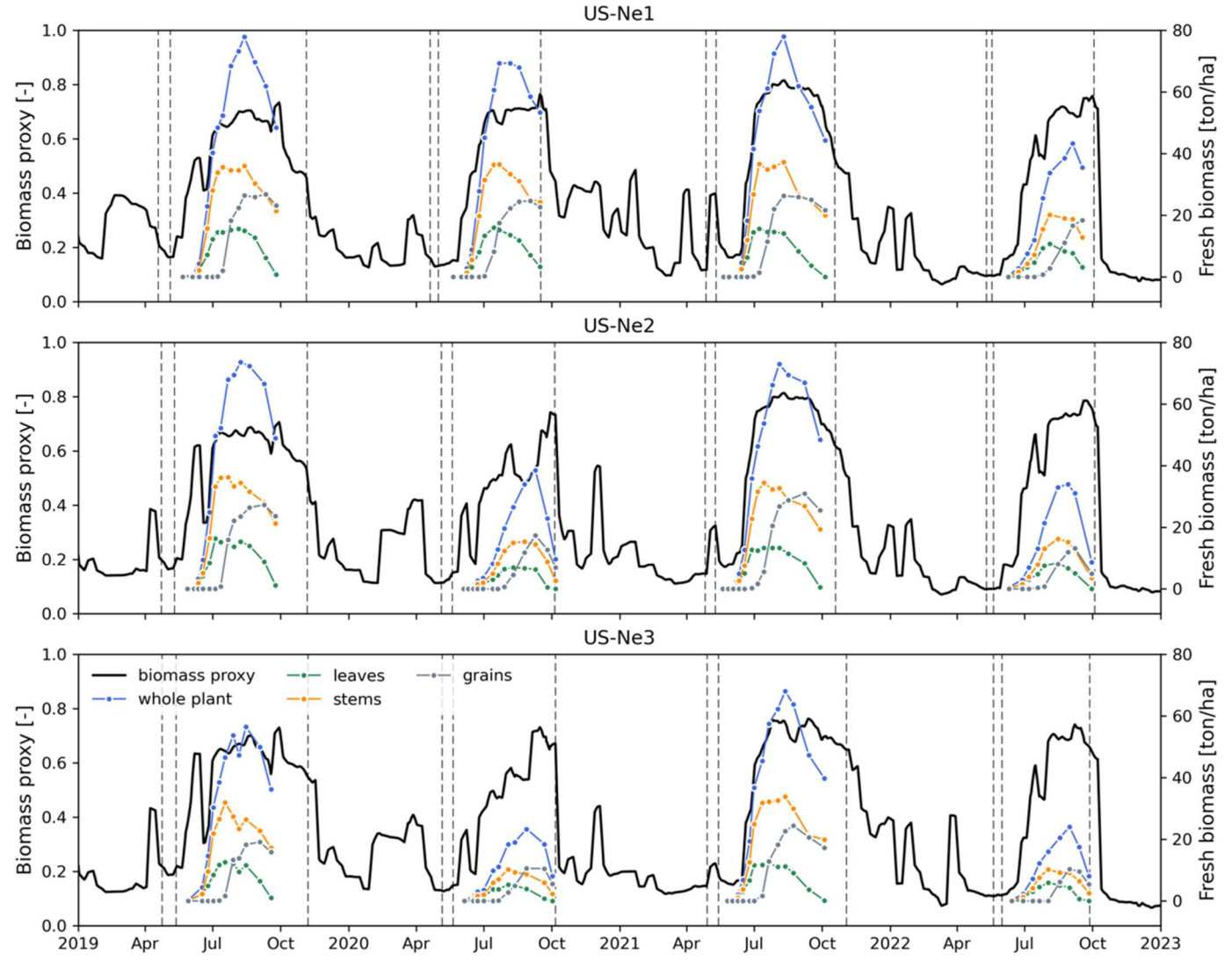


Fig. 7. Time series of satellite-based Biomass Proxy and aboveground fresh biomass components measured at the three sites in Mead, Nebraska (US-Ne1, US-Ne2, US-Ne3). Crop types are corn (2019, 2020 and 2021 at US-Ne1, 2019 and 2021 at US-Ne2 and US-Ne3) and soybean (2022 at US-Ne1, 2020 and 2022 at US-Ne2 and US-Ne3). US-Ne1 and US-Ne2 are irrigated fields, US-Ne3 is rainfed. Planting, emergence and harvest dates are represented with dashed vertical lines.

hectare for wheat in Michigan to 23 tons per hectare for corn in Nebraska. We noticed a clear change in the slope of the regression lines before and after a mean Biomass Proxy of around 0.5 (Fig. 12b) that might represent a mix of saturation and differences in crop variety. The saturation effect is mainly due to the attenuation of the signal through the canopy that at first approximation increases exponentially with the vegetation density (Attema and Ulaby, 1978). The harvest index represents the ratio between the total dry matter and grain yield that mainly depends on seed quality and environmental conditions and stresses (Hütsch and Schubert, 2017).

For individual crops, coefficients of determination were higher for corn, and the optimal integration period significantly varied from crop to crop. While describing the entire crop season for soybean, the optimal integration period was more representative of the plant vegetative phase and not accounting for the senescence phases of corn and wheat. For wheat, a significant sensitivity of the Biomass Proxy to wheat production was found before the heading stage that was estimated at around 1200 cumulative GDD. Similar results were described in previous studies (Mattia et al., 2003; Vreugdenhil et al., 2018; Wiseman et al., 2014), where the authors attributed the low explained variance in yield when accounting for the heading phase to the effect of the upper canopy structure rather than biomass accumulation. Wiegand et al. (1986)

showed that accounting for the plant senescence in the integrative period significantly reduced the correlations between crop yields and accumulated vegetation indices. For winter wheat, Fieuzal and Baup (2017) found best crop yield estimates ($R^2=0.76$) when accounting for radar polarimetric observations collected during the vegetative phase only, from leaves emergence to stem elongation.

3.4.2. Crop yield forecasting

The comparison between the three yield indicators clearly illustrated the better performance of indicators based on integrative periods rather than single observation/date such as the maximum of Biomass Proxy (Figs. 12 and 13) as already mentioned by Gorrab et al. (2021). On average, we found similar performance between the yield indicator based on the GDD-based integrative periods (R^2 =0.80) and the Biomass Proxy accumulation from emergence to the peak of Biomass Proxy (R^2 =0.78). The Biomass Proxy maximum was able to only explain a relatively low variance in crop yield with a coefficient of determination of around 0.2 and significantly higher relative MAE when accounting for all crops (rMAE=49 %).

Based on the field datasets available for this study, corn and soybean yields in Nebraska (17 and 6 tons per hectare on average, respectively) were higher than in Michigan (8 and 4 tons per hectare on average,

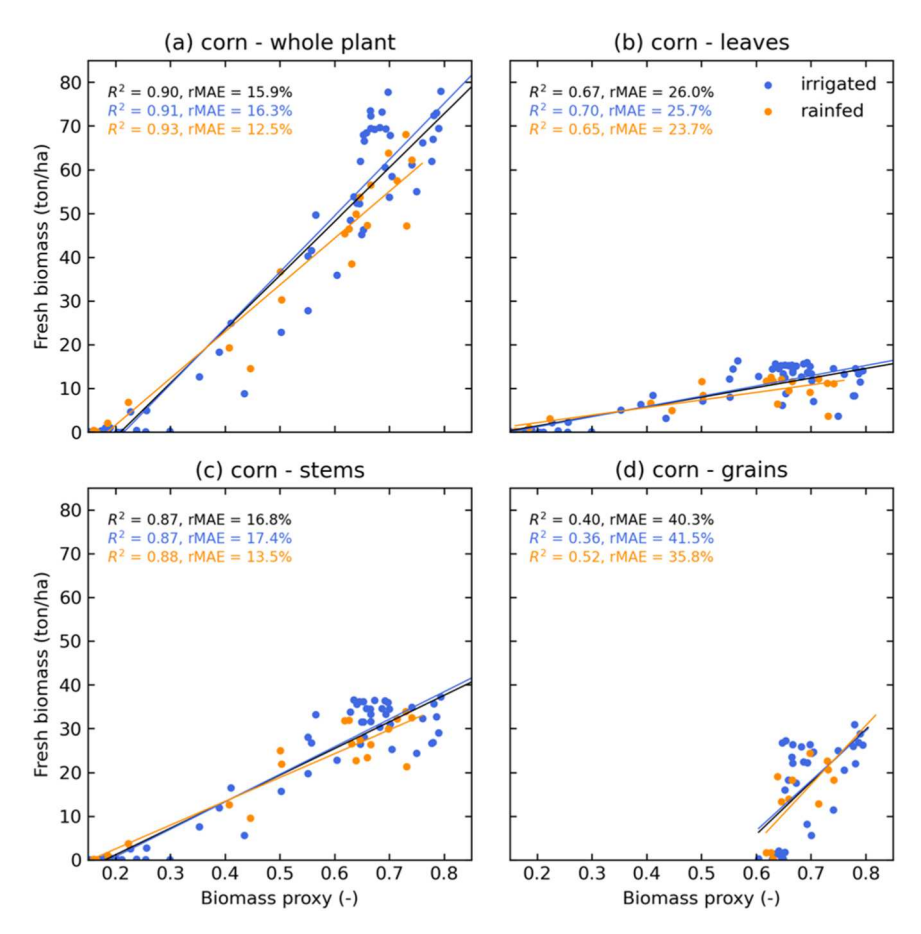


Fig. 8. Relationships between ground-based aboveground fresh biomass of the whole plant (a), leaves (b), stems (c) or grains (d), and satellite-derived Biomass Proxy products for corn fields near Mead, Nebraska. Correlations coefficients and relative MAE are calculated depending on water management, i.e., irrigated (blue dots) or rainfed fields (orange dots).

respectively). Both yield indicators based on integrated periods were able to clearly discriminate between different levels of production, whereas the maximum values of Biomass Proxy had no such capacity (Figs. 12 and 13). Fig. 13b and c clearly show the nonlinear relationship between the Biomass Proxy and crop yield with a large sensitivity at low values of yield and with a gradually decreasing sensitivity towards higher yield without reaching a clear saturation.

When analyzing the regressions site by site, we found that the yield indicator defined as the mean Biomass Proxy from emergence to maximum value through the season was providing in most cases the highest correlations and lowest relative MAE (Fig. 14). In Nebraska, the Biomass Proxy was able to clearly describe the differences in yield between rainfed and irrigated soybean (Fig. 14a) but in a less obvious way for corn. Results might reflect the differences observed in ground-based biomass measurements between rainfed and irrigated crops. First, ground-based measurements showed that the main differences between rainfed and irrigated crop biomass were mainly due to stem and grain biomass for soybean and only to grain biomass for corn (Fig. 3), and we have already shown that the biomass proxy was highly sensitive to variations in stem biomass and much less so to grain biomass for both corn and soybean (Figs. 8 and 9). Moreover, grains grow after the vegetative phase, when the canopy is fully developed, and differences in corn grain biomass might have a reduced influence on the Biomass Proxy due to saturation effects. For corn, individual plant data was used to calculate the standard error (SE) of the mean and assess the reliability of IMZ mean yield values based on the experimental sampling which is represented by error bars in Fig. 14.

In Michigan, the Biomass Proxy was able to measure the different yield levels of corn fields associated with various management treatments with a R² of around 0.5 and relative MAE varying from 13 % for corn, 17 % for soybean and 21 % for wheat (Fig. 14b). For corn, mean Biomass Proxy varied from 0.33 to 0.65 when yield varied from 6 to 11 tons per hectare. Results were less obvious for soybean and wheat since the yields associated with T1, T2 and T3 treatments were similar. However, for each crop, the Biomass Proxy was able to clearly discriminate the low yield levels of the biologically treated fields (T4 treatment) (Figs. 14b and 15) from the other treatments. It should be noted that the regression lines related to the different crops were distinct with similar slopes but different intercepts, i.e., where the regression line intersected the *y*-axis. As mentioned by Mattia et al. (2003), observed differences might be explained by differences in the structure of the crop canopy that affect the scattering processes.

4. Discussion

Since the launch of Sentinel 1 by ESA, SAR data has been increasingly used to monitor agricultural systems. However, the relative complexity associated with the processing and interpretation of radar images compared to optical data, could explain why most radar applications are exploratory and in the fields of research (Liu et al., 2019; Steele-Dunne et al., 2017). In this paper, we demonstrated that the Biomass Proxy, fusing information from Sentinel-1 and Sentinel-2, can provide a valuable analysis ready data to help monitor the aboveground biomass of crops throughout the growing season and provide early assessments of crop yield. The ability of the Biomass Proxy to measure agricultural systems repeatedly during the crop growth cycles independently of cloud coverage conditions is an added advantage for operational agricultural management purposes.

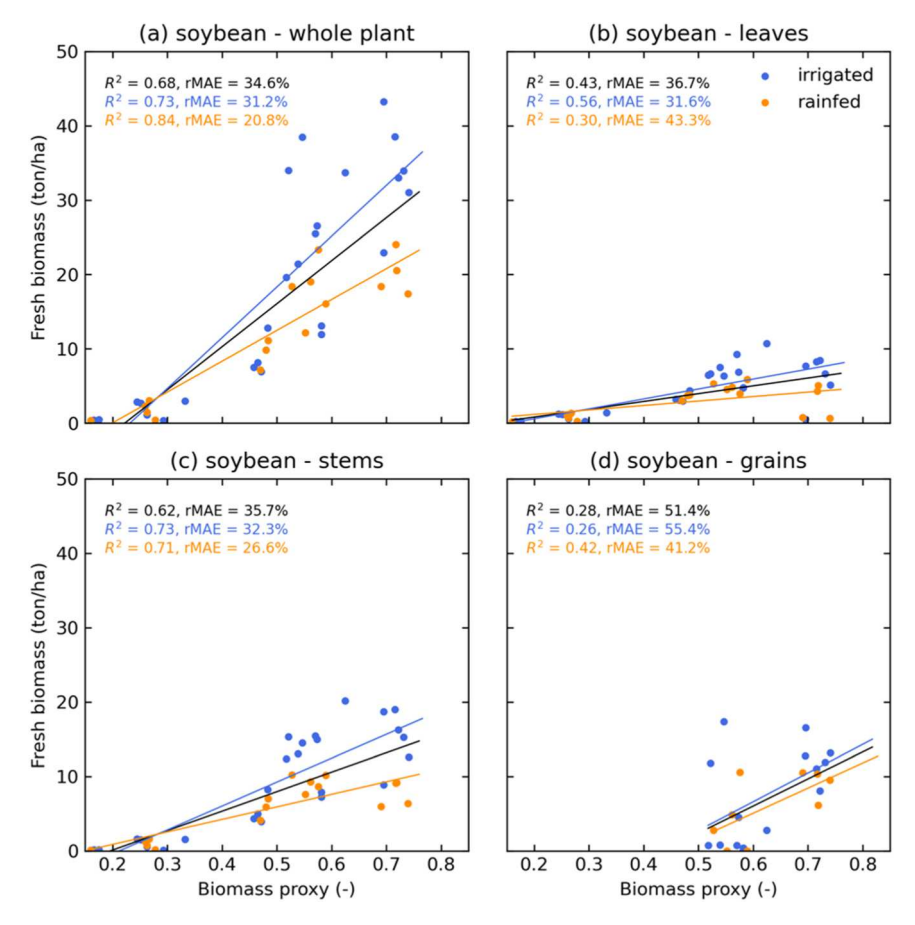


Fig. 9. Relationships between ground-based aboveground fresh biomass of the whole plant (a), leaves (b), stems (c) or grains (d), and satellite-derived Biomass Proxy products for soybean fields near Mead, Nebraska. Correlations coefficients and relative MAE are calculated depending on water management, i.e., irrigated (blue dots) or rainfed fields (orange dots).

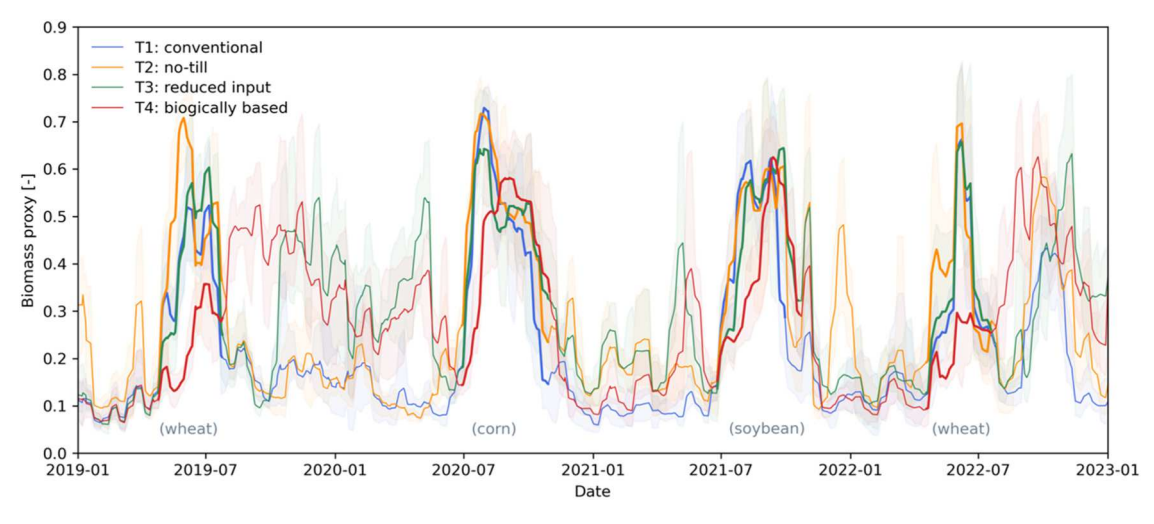


Fig. 10. Time series of Biomass Proxy describing relative biomass of crops at the Kellogg station associated with different treatments, i.e., Michigan conventional (T1), no till (T2), reduced chemical inputs (T3) and biologically based (T4). For each treatment, the solid light line represents the mean Biomass Proxy over six replicated fields whose variations are shown by faded envelopes of time series, and the solid thick line represents the crop season from emergence to harvest.

4.1. Biomass Proxy to monitor crop fresh biomass

Based on ground-based measurements carried out in corn and soybean fields near Mead, Nebraska, we found very good agreements between time series of Biomass Proxy time series and fresh biomass. Results clearly demonstrated that the Biomass Proxy can serve as a good indicator of crop growth status ($R^2>0.9$ for corn and $R^2>0.7$ for soybean) and was able to robustly detect variations in biomass accumulation due to agricultural management or environmental conditions. We observed higher correlations with total plant and stem fresh biomass compared to leaf biomass. Findings were consistent with earlier research. Using a C-band ground radar, Mattia et al. (2003) found poor

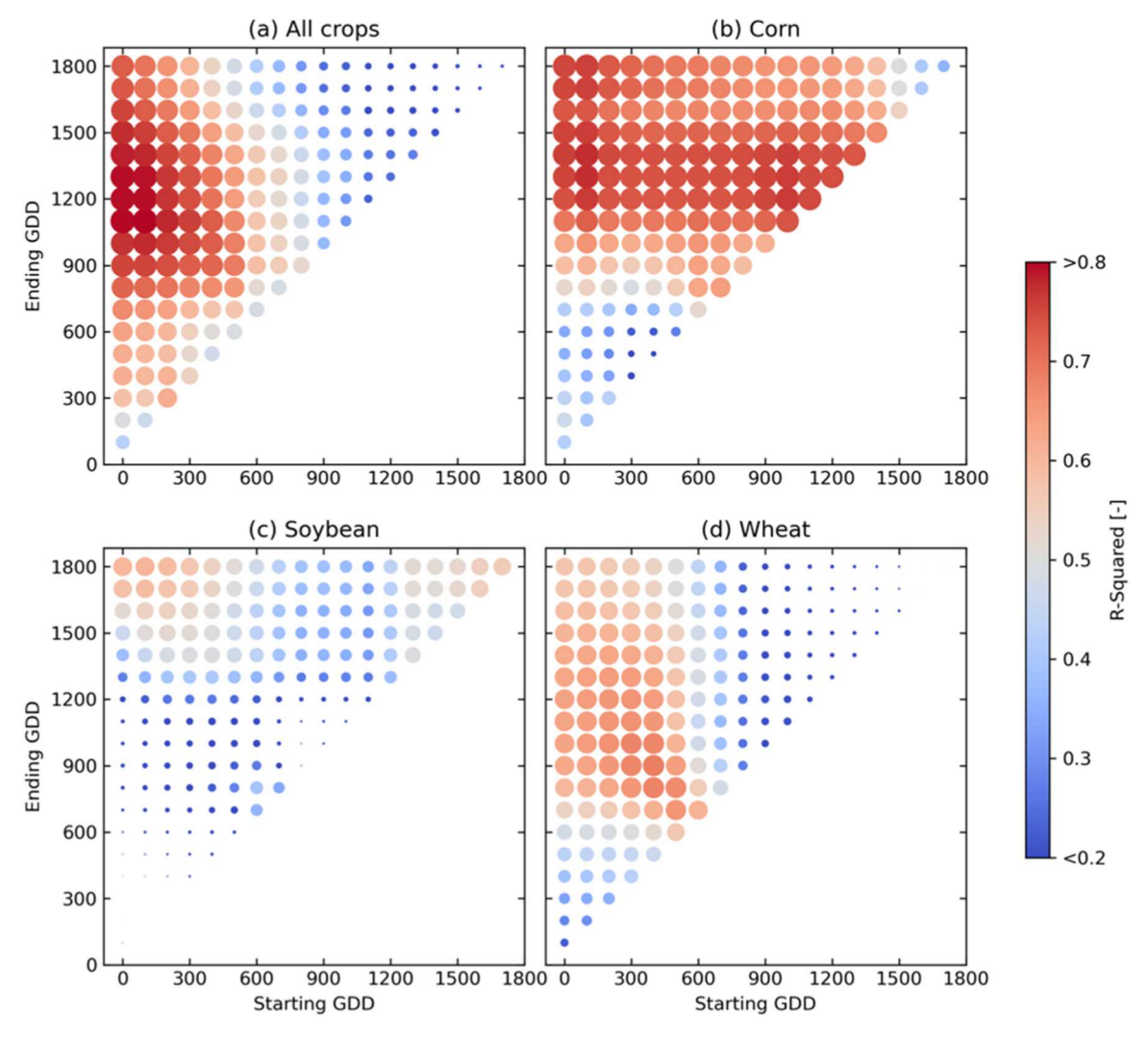


Fig. 11. Coefficients of determination R² between the mean Biomass Proxy over various periods of time through the crop season and crop yield accounting for all crops (a), corn (b), soybean (c) and wheat (d). Both size and color of the markers represent R² based on exponential regression models.

Table 2 GDD-based integration periods associated with the highest coefficient of determination (\mathbb{R}^2) and lowest relative MAE between Biomass Proxy mean values and crop yield when considering all available matchup data from the Mead, Nebraska and Kellogg, Michigan experiments. The GDD-based integration periods are defined by starting and ending cumulative GDD after crop emergence (Fig. 4). Linear and regression models were evaluated.

	Crop type	Starting GDD_C	Ending GDD_C	\mathbb{R}^2	rMAE
Linear	All crops	0	1200	0.704	30.4 %
regressions	Corn	100	1400	0.796	13.6 %
	Soybean	100	1800	0.603	18.1 %
	Wheat	400	900	0.686	15.6 %
Exponential	All crops	100	1100	0.801	23.1 %
regressions	Corn	100	1400	0.781	14.5 %
	Soybean	100	1800	0.580	18.4 %
	Wheat	400	900	0.564	18.2~%

correlations between the fresh biomass of the leaves and all the other plant components (e.g., total plant, stem or ear biomass, plant height). Using Sentinel 1, Vreugdenhil et al. (2018) showed that the cross ratio was able to account for 87 % of the variability in vegetation water content for corn and found lower correlations for other crop types, e.g., \mathbb{R}^2 of 0.63 and 0.34 for wheat and oil seed respectively. As already

mentioned in the results section, we noticed a saturation of the Biomass Proxy for high values of fresh biomass of around 55–60 tons per hectare for corn, which corresponded to LAI values between 4 and 5. Saturation effects means that as a crop is accumulating biomass through the vegetative phase, the Biomass Proxy will lose sensitivity to additional fresh matter after a certain level of accumulated biomass, which is crop and frequency dependent. Reflected signals in the optical domain usually reach saturation before radar backscattered coefficients because they have a reduced penetration length through the canopy. Likewise, C-band SAR data may saturate before L-band. Similar saturation effects on SAR acquisitions have been reported in many previous studies (Steele-Dunne et al., 2017). Using airborne data over corn fields, Ferrazzoli et al. (1992) found that C- and S-band VV and HH polarizations saturated for LAI between 2 and 3 for example.

Regarding the effect of irrigation on the relationships between the Biomass Proxy and crop biomass, we observed that the relative differences between total fresh biomass of irrigated and rainfed fields, which were higher for soybean than for corn (see Figs. 3, 8 and 9) had a relatively low influence on the Biomass Proxy. This could be due to multiple factors. First, unlike corn, both VH and VV backscatter coefficients over soybean are influenced by volume scattering, which reduces the impact of a change in vegetation density on the ratio VH/VV and the Biomass Proxy. In addition, until the soybean canopy is closed, Biomass Proxy represents a mixed signal between vegetation and soil

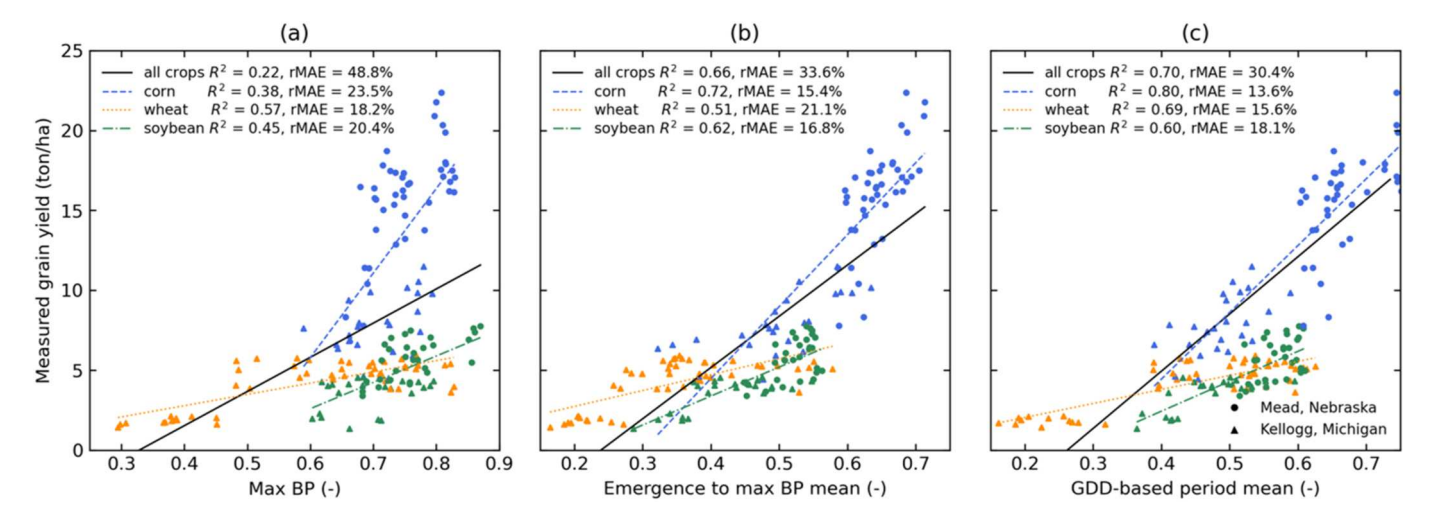


Fig. 12. Relationships between crop yield and three different yield indicators based on time series of Biomass Proxy (BP): the maximum value of BP through the crop season (a), the mean values of BP from crop emergence to BP max (b) and the mean value of BP over GDD-based integration periods defined in Table 1 (c). R² and relative MAE values are based on linear regression models. The analysis included data from both sites.

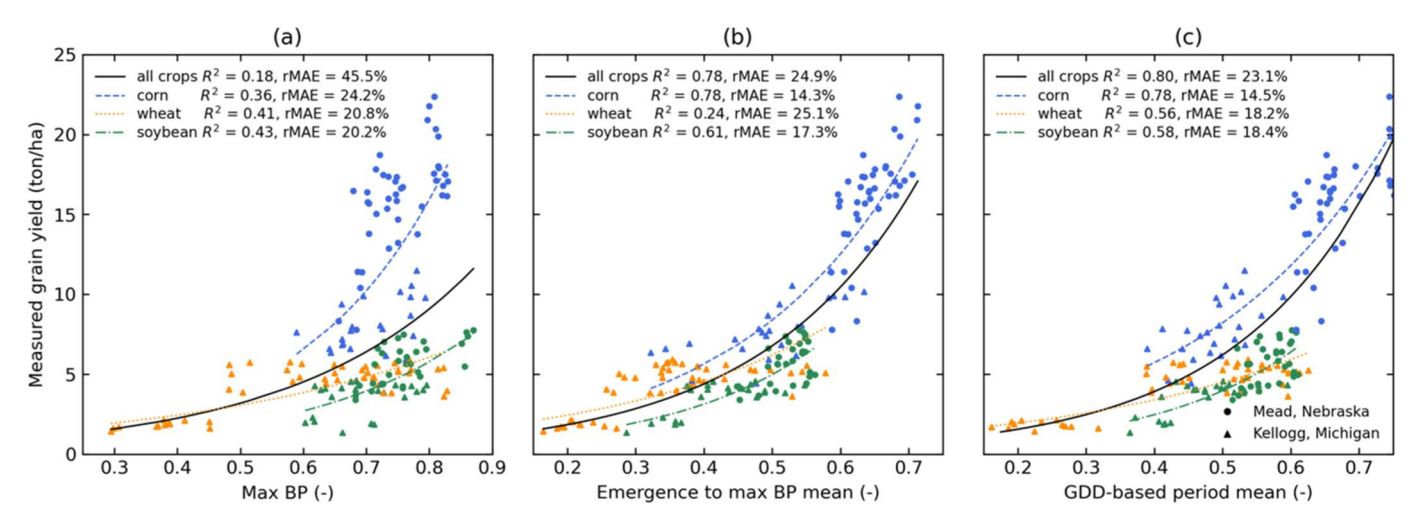
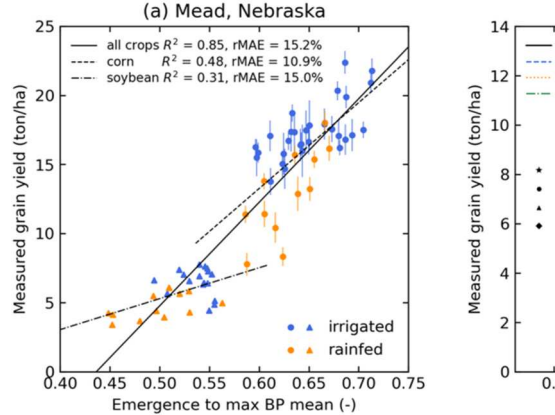


Fig. 13. Relationships between crop yield and three different yield indicators based on time series of Biomass Proxy (BP): the maximum value of BP through the crop season (a), the mean values of BP from crop emergence to BP max (b) and the mean value of BP over GDD-based integration periods defined in Table 1 (c). R2 and relative MAE values are based on exponential regression models. The analysis included data from both sites.

contributions, and the contribution of the vegetation might saturate at relatively low field LAI due to the fact that the vegetation components were concentrated into rows. When leaves are arranged in rows, vegetation density is locally higher compared to if the same number of leaves were uniformly distributed across a vegetation layer. The saturation effect is influenced by the canopy structure and the incidence angle. A reduction in the canopy cover fraction leads to a decrease in the LAI value at which saturation occurs (Guillevic et al., 2003). We did not have enough measurements of soybean fresh biomass to statistically verify these hypotheses. In Fig. 9, we observed a significant difference in the slope of the regression lines of rainfed and irrigated soybean fields, while the regression lines for corn were similar with or without irrigation (Fig. 8). The difference in slope between corn and soybean could be due to several factors, such as changes in canopy structure due to water stress or saturation effects which could be enhanced by the row structure of soybean canopies. In such a case, the Biomass Proxy could be more responsive to changes in growth stage, such as the size of the plant and associated canopy coverage, rather than biomass accumulation. A rigorous interpretation of the observed differences would require further research and additional information on canopy structure, which were not available for this study.

4.2. Biomass Proxy to early assess crop yield

Both datasets collected at Mead and Kellogg were used to demonstrate the ability of Biomass Proxy to assess final yield early in the season. We found good agreements between crop yield and the Biomass Proxy when using average Biomass Proxy through periods of time describing the crop vegetative phase (R2 around 0.8). Similar results were reported by past studies based on remote sensing data in the short wave and microwave spectral domains (Fieuzal and Baup, 2017; Gao et al., 2018; Gorrab et al., 2021; Wiegand et al., 1986). Yield indicators based on maximum Biomass Proxy through the growing season were less efficient mainly due to saturation effects over dense vegetation. When considering all crops, we found that the Biomass Proxy could be used to assess crop yield 6-8 weeks before harvest, when crop biomass may still improve in response to curative actions such as fertilization or irrigation. However, with such a design, if an anomaly in crop development occurred after the plant vegetative phase, its effect on final yield might not be accounted for by the average Biomass Proxy. As field observations that describe all possible effects of environmental stresses (e.g., water stress, nitrogen deficit, pest diseases) on yield must be fastidious and at present do not exist, operational management might require an optimal



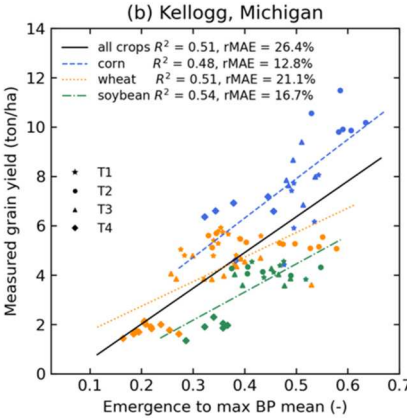


Fig. 14. Relationships between crop yield and Biomass Proxy (BP) products at Mead, Nebraska (a) and Kellog, Nebraska (b). BP-based yield indicators represent the mean BP value through the vegetative phase calculated between the plant emergence and the maximum value of BP. R^2 and relative MAE values are based on linear regression models. Data was collected during four crop seasons from 2019 to 2022. (a) Data represent irrigated (blue markers) and rainfed (orange markers) corn (circle markers) and soybean (triangle markers). The errors bars represent \pm one standard error around the mean derived from measurement replicates made over corn IMZs. (b) Data represents corn (blue markers), soybean (green markers) and wheat (orange markers) associated with four different treatments, i.e., Michigan conventional (T1), no till (T2), reduced chemical inputs (T3) and biologically based (T4), are considered for each crop.

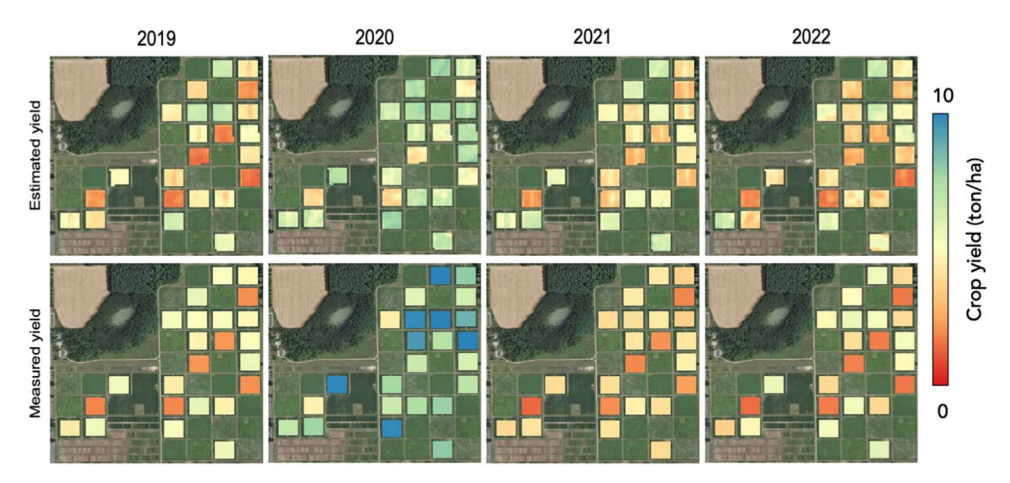


Fig. 15. Maps of crop yield measured in situ at Kellogg Biological Station, Michigan (bottom row) and derived from the Biomass Proxy using a linear regression model (see Table 1) (top row). Three different crops are represented: wheat (2019 and 2022), corn (2020) and soybean (2021).

tradeoff between yield estimate uncertainties and relevant integration periods that should include all phenological phases for which any stress would have an impact on yield. We also found that winter wheat yield was associated with higher relative errors (rMAE=21 %) than corn (13 %) and soybean (17 %) as already observed by Wiseman et al. (2014) using different polarimetric parameters based on Radarsat-2 or by Chaparro et al. (2018) at a coarser spatial resolution using VOD products derived from L-band SMAP observations. Using optical data at moderate resolution, Franch et al. (2021) estimated wheat yield at county levels with uncertainties up to 20 %.

For each crop in Michigan, Biomass Proxy was clearly able to differentiate low yield fields associated with biological treatments (T4) and most productive fields that received the conventional with no till treatment (T2). The relative differences in Biomass Proxy based yield indicator values between T4 and T2 treatments were around 70 %, 60 % and 50 % for corn, soybean, and wheat, respectively. The corresponding relative differences in yield values between T4 and T2 treatments were similar and around 80 %, 50 % and 40 % for corn, soybean, and wheat, respectively. Such differences between T2 and T4 treatments were mainly due to nitrogen deficit, especially for wheat fields that were immediately following the harvest of soybean, which left little nitrogenrich residue for the following crop, compared to corn that followed winter wheat (Philip Robertson et al., 2014). For corn in 2020, the

Biomass Proxy and yields of the T2 no-till treatment fields were 20 % and 30 %, respectively, higher than they were in the conventional system. On average, Philip Robertson et al. (2014) reported differences in yields between T2 and T1 treatments of around 9–20 % depending on the year and drought status. The higher difference observed in 2020 (30 %) might be due to a significant drought event that occurred in Michigan in 2020 and clearly illustrated the enhanced water storage capacity of no-till systems compared to conventional practices that translated in lower water stress and higher productivity. Results demonstrated the ability of the Biomass Proxy to detect the effect of water shortage on yield by comparing current observations with a Biomass Proxy normal baseline representing average Biomass Proxy over the years or a reference year for which satellite response and yield are known.

As shown in this paper, monitoring crop biomass using Biomass Proxy or SAR systems in general depends on multiple parameters describing a crop and its environment. For a given cultivar, the yield prediction method based on GDD-derived integration periods could be applied across regions with disparate climates. However, cultivars with different phenological development characteristics may reach maturity at varying cumulative GDD, which may influence the yield model. In this study, we were able to characterize the model for three different crops, i. e., corn, wheat and soybean; however, we lacked sufficient data to assess

the impact of different cultivars. Therefore, the empirical relationships between the Biomass Proxy and crop biomass described here may not be easily scalable to different crop types, regions, and environmental conditions.

For decision making support, additional field surveys and research are needed to generalize our findings and derive standard yield retrievals. Moreover, the quality of the retrieval relationships depends on the representativity and accuracy of the field validation datasets, which are also subject to uncertainties due to the intra field spatial variability and the sampling design. In our study for instance, the fields are managed by different farm operators with specific agricultural practices and experimental designs such as field sampling and biomass measurement protocols. In Mead, Nebraska, yield data representing a 30×30 m² IMZ area were based on samples of around 7 and 30 plants for corn and soybean, respectively. We found an average relative standard error of 6.4 % of the assessed corn yield, characterizing additional uncertainties due to the field measurement protocol. In Kellogg, Michigan, yield data were based on combine measurements and were fully representative of the entire field and the satellite product footprint. Uncertainties are also associated with the Biomass Proxy that does not directly correlate with crop yield, i.e., the dry biomass of the grains. Instead, Biomass Proxy is related to the fresh biomass of the plant components involved in the scattering and attenuation radiometric mechanisms, which may correspond to different parts of the crop depending on the crop type and the phenological stage. A full characterization of the different sources of uncertainties was not possible in this study and would need additional measurements and further research.

5. Conclusion

This study demonstrated the potential of Planet's Biomass Proxy product to monitor vegetation dynamics and assess crop production. Field validation datasets collected at Mead, Nebraska and Kellogg Biological Station by the University of Nebraska-Lincoln and Michigan State University, respectively, were used to evaluate the relationships between the Biomass Proxy and the biomass of corn, winter wheat and soybean fields. Time series analysis clearly illustrated the sensitivity of the Biomass Proxy product to changes in crop fresh biomass (i.e., plant water content) through the growing season, which showcased the potential of the Biomass Proxy to detect rapid changes in plant growth due to agricultural practices or environmental stresses, such as nitrogen deficit or water stress. The Biomass Proxy was highly correlated with the fresh biomass of corn ($R^2 > 0.9$) and soybean (R^2 around 0.7) allowing near real time monitoring of crop growth. Using an exponential regression model, the Biomass Proxy was able to explain 80 % of the yield variance of agricultural fields consisting of corn, winter wheat and soybean one to two months before harvest, allowing decision to be made regarding the need for additional inputs. We have shown that the Biomass Proxy can provide essential support for crop management, especially over cloudy regions where no other remote source of information is frequently available. The product is expected to be helpful in characterizing crop dynamic processes and mitigating the impact of climate variability on agriculture by providing information on plant growth status and response to environmental stresses. Further research will focus on the use of bundled Planet's Planetary Variables, i.e. Biomass Proxy, Soil Water Content and Land Surface Temperature, and Planet's Analysis Ready Data Surface Reflectance products (Houborg and McCabe, 2018a, 2018b, 2018c) to monitor crop growth and forecast yield.

CRediT authorship contribution statement

G. Philip Robertson: Resources. **Richard De Jeu:** Writing – review & editing, Project administration. **Pierre C. Guillevic:** Writing – original draft, Visualization, Software, Methodology, Investigation, Data curation, Conceptualization. **Benjamin Aouizerats:** Visualization,

Methodology, Data curation, Conceptualization. Rogier Burger: Writing – review & editing, Methodology, Investigation. Nadja den Besten: Writing – review & editing, Investigation. Daniel Jackson: Writing – review & editing, Investigation. Margot Ridderikhoff: Writing – review & editing, Investigation. Ariel Zajdband: Writing – review & editing, Resources. Rasmus Houborg: Writing – review & editing, Resources. Trenton E. Franz: Writing – review & editing, Resources.

Declaration of Competing Interest

The authors declare that they have no known competing financial interests or personal relationships that could have appeared to influence the work reported in this paper.

Data availability

Data will be made available on request.

Acknowledgements

We acknowledge the contribution of ground-based research data from the Carbon Sequestration Project at the University of Nebraska-Lincoln and the Kellogg Biological Station at Michigan State University. In addition, support for field experiments was also provided by the NSF Long-term Ecological Research Program (DEB 2224712) at the Kellogg Biological Station and by Michigan State University AgBioResearch. Funding for the AmeriFlux core sites at the Eastern Nebraska Research Education and Extension Center was provided by the U.S. Department of Energy's Office of Science. This research was a contribution from the Long-Term Agroecosystem Research (LTAR) network. LTAR is supported by the United States Department of Agriculture. T.E. F. acknowledges the financial support of the USDA National Institute of Food and Agriculture, Hatch projects #1009760, #1020768 and #2023-67021-38977. The findings and views described herein do not necessarily reflect those of Planet Labs PBC.

References

- Attema, E.P.W., Ulaby, F.T., 1978. Vegetation modeled as a water cloud. Radiol. Sci. 13, 357–364. https://doi.org/10.1029/RS013i002p00357.
- Baetens, L., Desjardins, C., Hagolle, O., 2019. Validation of copernicus sentinel-2 cloud masks obtained from MAJA, Sen2Cor, and FMask processors using reference cloud masks generated with a supervised active learning procedure. Remote Sen.s 11, 433. https://doi.org/10.3390/rs11040433.
- Baldocchi, D., Falge, E., Gu, L., Olson, R., Hollinger, D., Running, S., Anthoni, P., Bernhofer, C., Davis, K., Evans, R., Fuentes, J., Goldstein, A., Katul, G., Law, B., Lee, X., Malhi, Y., Meyers, T., Munger, W., Oechel, W., Paw, K.T., Pilegaard, K., Schmid, H.P., Valentini, R., Verma, S., Vesala, T., Wilson, K., Wofsy, S., 2001. FLUXNET: a new tool to study the temporal and spatial variability of ecosystem–scale carbon dioxide, water vapor, and energy flux densities. Bull. Am. Meteorol. Soc. 82, 2415–2434. https://doi.org/10.1175/1520-0477(2001) 082-2415-EANTTS-2-3 CO2
- Basso, B., Liu, L., 2019. Seasonal crop yield forecast: methods, applications, and accuracies. In: Advances in Agronomy. Elsevier, pp. 201–255. https://doi.org/ 10.1016/bs.agron.2018.11.002.
- Becker-Reshef, I., Barker, B., Humber, M., Puricelli, E., Sanchez, A., Sahajpal, R., McGaughey, K., Justice, C., Baruth, B., Wu, B., Prakash, A., Abdolreza, A., Jarvis, I., 2019. The GEOGLAM crop monitor for AMIS: assessing crop conditions in the context of global markets. Glob. Food Secur. 23, 173–181. https://doi.org/10.1016/j.gfs.2019.04.010.
- Becker-Reshef, I., Vermote, E., Lindeman, M., Justice, C., 2010. A generalized regression-based model for forecasting winter wheat yields in Kansas and Ukraine using MODIS data. Remote Sens. Environ. 114, 1312–1323. https://doi.org/10.1016/j.rse.2010.01.010.
- den Besten, N., Steele Dunne, S., Mahmud, A., Jackson, D., Aouizerats, B., de Jeu, R., Burger, R., Houborg, R., McGlinchey, M., van der Zaag, P., 2023. Understanding Sentinel-1 backscatter response to sugarcane yield variability and waterlogging. Remote Sens. Environ. 290, 113555 https://doi.org/10.1016/j.rse.2023.113555.
- Bouvet, A., Thuy Le Toan, Dao, N.L., 2014. Estimation of agricultural and biophysical parameters of rice fields in Vietnam using X-band dual-polarization SAR. In: 2014 IEEE Geoscience and Remote Sensing Symposium. Presented at the IGARSS 2014 2014 IEEE International Geoscience and Remote Sensing Symposium. IEEE, Quebec City, QC, pp. 1504–1507. https://doi.org/10.1109/IGARSS.2014.6946723.

- Brisco, B., Brown, R., Koehler, J., Sofko, G., Mckibben, M., 1990. The diurnal pattern of microwave backscattering by wheat. Remote Sens. Environ. 34, 37–47. https://doi. org/10.1016/0034-4257(90)90082-W.
- Burger, R., Aouizerats, B., Den Besten, N., Guillevic, P., Catarino, F., Van Der Horst, T., Jackson, D., Koopmans, R., Ridderikhoff, M., Robson, G., Zajdband, A., De Jeu, R., 2024. The biomass proxy: unlocking global agricultural monitoring through fusion of sentinel-1 and sentinel-2. Remote Sens 16, 835. https://doi.org/10.3390/rs16050835
- Chaparro, D., Piles, M., Vall-Ilossera, M., Camps, A., Konings, A.G., Entekhabi, D., 2018. L-band vegetation optical depth seasonal metrics for crop yield assessment. Remote Sens. Environ. 212, 249–259. https://doi.org/10.1016/j.rse.2018.04.049.
- Chen, C., Mcnairn, H., 2006. A neural network integrated approach for rice crop monitoring. Int. J. Remote Sens. 27, 1367–1393. https://doi.org/10.1080/ 01431160500421507.
- d'Andrimont, R., Verhegghen, A., Lemoine, G., Kempeneers, P., Meroni, M., van der Velde, M., 2021. From parcel to continental scale – a first European crop type map based on Sentinel-1 and LUCAS Copernicus in-situ observations. Remote Sens. Environ. 266, 112708 https://doi.org/10.1016/j.rse.2021.112708.
- Daughtry, C.S.T., Gallo, K.P., Bauer, M.E., 1983. Spectral Estimates of Solar Radiation Intercepted by Corn Canopies ¹. Agron. J. 75, 527–531. https://doi.org/10.2134/agronj1983.00021962007500030026x.
- Deschamps, B., McNairn, H., Shang, J., Jiao, X., 2012. Towards operational radar-only crop type classification: comparison of a traditional decision tree with a random forest classifier. Can. J. Remote Sens. 38, 60–68. https://doi.org/10.5589/m12-012.
- El Hajj, M., Baghdadi, N., Wigneron, J.-P., Zribi, M., Albergel, C., Calvet, J.-C., Fayad, I., 2019. First Vegetation Optical Depth Mapping from Sentinel-1 C-band SAR Data over Crop Fields. Remote Sens 11, 2769. https://doi.org/10.3390/rs11232769.
- El Hajj, M.M., Johansen, K., Almashharawi, S.K., McCabe, M.F., 2023. Water uptake rates over olive orchards using Sentinel-1 synthetic aperture radar data. Agric. Water Manag. 288, 108462 https://doi.org/10.1016/j.agwat.2023.108462.
- FAO, 2022. The future of food and agriculture Drivers and triggers for transformation.
 Ferrazzoli, P., Paloscia, S., Pampaloni, P., Schiavon, G., Solimini, D., Coppo, P., 1992.
 Sensitivity of microwave measurements to vegetation biomass and soil moisture content: a case study. IEEE Trans. Geosci. Remote Sens. 30, 750–756. https://doi.org/10.1109/36.158869.
- Fieuzal, R., Baup, F., 2017. Forecast of wheat yield throughout the agricultural season using optical and radar satellite images. Int. J. Appl. Earth Obs. Geoinf. 59, 147–156. https://doi.org/10.1016/j.jag.2017.03.011.
- Franch, B., Vermote, E., Skakun, S., Santamaria-Artigas, A., Kalecinski, N., Roger, J.-C., Becker-Reshef, I., Barker, B., Justice, C., Sobrino, J.A., 2021. The ARYA crop yield forecasting algorithm: Application to the main wheat exporting countries. Int. J. Appl. Earth Obs. Geoinf. 104, 102552 https://doi.org/10.1016/j.jag.2021.102552.
- Franz, T.E., Pokal, S., Gibson, J.P., Zhou, Y., Gholizadeh, H., Tenorio, F.A., Rudnick, D., Heeren, D., McCabe, M., Ziliani, M., Jin, Z., Guan, K., Pan, M., Gates, J., Wardlow, B., 2020. The role of topography, soil, and remotely sensed vegetation condition towards predicting crop yield. Field Crops Res 252, 107788. https://doi.org/10.1016/j.fcr.2020.107788.
- Funk, C., Budde, M.E., 2009. Phenologically-tuned MODIS NDVI-based production anomaly estimates for Zimbabwe. Remote Sens. Environ. 113, 115–125. https://doi. org/10.1016/j.rse.2008.08.015.
- Gao, F., Anderson, M., Daughtry, C., Johnson, D., 2018. Assessing the variability of corn and soybean yields in central iowa using high spatiotemporal resolution multisatellite imagery. Remote Sens. 10, 1489. https://doi.org/10.3390/rs10091489.
 Gascon, F., Bouzinac, C., Thépaut, O., Jung, M., Francesconi, B., Louis, J., Lonjou, V.,
- Gascon, F., Bouzinac, C., Thépaut, O., Jung, M., Francesconi, B., Louis, J., Lonjou, V., Lafrance, B., Massera, S., Gaudel-Vacaresse, A., Languille, F., Alhammoud, B., Viallefont, F., Pflug, B., Bieniarz, J., Clerc, S., Pessiot, L., Trémas, T., Cadau, E., De Bonis, R., Isola, C., Martimort, P., Fernandez, V., 2017. Copernicus Sentinel-2A Calibration and Products Validation Status. Remote Sens. 9, 584. https://doi.org/10.3390/rs9060584.
- Gorrab, A., Ameline, M., Albergel, C., Baup, F., 2021. Use of Sentinel-1 Multi-Configuration and Multi-Temporal Series for Monitoring Parameters of Winter Wheat. Remote Sens. 13, 553. https://doi.org/10.3390/rs13040553.
- Guillevic, P., Gastellu-Etchegorry, J.P., Demarty, J., Prevot, L., 2003. Thermal infrared radiative transfer within three-dimensional vegetation covers. J. Geophys. Res. 108, 4248. https://doi.org/10.1029/2002JD002247.
- Harfenmeister, K., Spengler, D., Weltzien, C., 2019. Analyzing TEmporal and Spatial Characteristics of Crop Parameters Using Sentinel-1 Backscatter Data. Remote Sens. 11, 1569. https://doi.org/10.3390/rs11131569.
- Hatfield, J.L., Cryder, M., Basso, B., 2020. Remote Sensing: Advancing the Science and the Applications to Transform Agriculture. IT Prof. 22, 42–45. https://doi.org/ 10.1109/MITP.2020.2986102.
- Hersbach, H., Bell, B., Berrisford, P., Hirahara, S., Horányi, A., Muñoz-Sabater, J.,
 Nicolas, J., Peubey, C., Radu, R., Schepers, D., Simmons, A., Soci, C., Abdalla, S.,
 Abellan, X., Balsamo, G., Bechtold, P., Biavati, G., Bidlot, J., Bonavita, M., Chiara, G.,
 Dahlgren, P., Dee, D., Diamantakis, M., Dragani, R., Flemming, J., Forbes, R.,
 Fuentes, M., Geer, A., Haimberger, L., Healy, S., Hogan, R.J., Hólm, E.,
 Janisková, M., Keeley, S., Laloyaux, P., Lopez, P., Lupu, C., Radnoti, G., Rosnay, P.,
 Rozum, I., Vamborg, F., Villaume, S., Thépaut, J., 2020. The ERA5 global reanalysis.
 Q. J. R. Meteorol. Soc. 146, 1999–2049. https://doi.org/10.1002/qj.3803.
- Houborg, R., McCabe, M.F., 2018b. A Cubesat enabled Spatio-Temporal Enhancement Method (CESTEM) utilizing Planet, Landsat and MODIS data. Remote Sens. Environ. 209, 211–226. https://doi.org/10.1016/j.rse.2018.02.067.
- Houborg, R., McCabe, M.F., 2018c. A hybrid training approach for leaf area index estimation via Cubist and random forests machine-learning. ISPRS J. Photogramm. Remote Sens. 135, 173–188. https://doi.org/10.1016/j.isprsjprs.2017.10.004.

- Houborg, R., McCabe, M., 2018a. Daily Retrieval of NDVI and LAI at 3 m resolution via the fusion of CubeSat, Landsat, and MODIS Data. Remote Sens 10, 890. https://doi.org/10.3390/rs10060890.
- Hütsch, B.W., Schubert, S., 2017. Harvest Index of Maize (Zea mays L.): Are There Possibilities for Improvement?. In: Advances in Agronomy. Elsevier, pp. 37–82. https://doi.org/10.1016/bs.agron.2017.07.004.
- Jiao, X., McNairn, H., Shang, J., Pattey, E., Liu, J., Champagne, C., 2011. The sensitivity of RADARSAT-2 polarimetric SAR data to corn and soybean leaf area index. Can. J. Remote Sens. 37, 69–81. https://doi.org/10.5589/m11-023.
- Karam, M.A., Fung, A.K., Lang, R.H., Chauhan, N.S., 1992. A microwave scattering model for layered vegetation. IEEE Trans. Geosci. Remote Sens. 30, 767–784. https://doi.org/10.1109/36.158872.
- Kim, Y., Jackson, T., Bindlish, R., Lee, Hoonyol, Hong, Sukyoung, 2012. Radar vegetation index for estimating the vegetation water content of rice and soybean. IEEE Geosci. Remote Sens. Lett. 9, 564–568. https://doi.org/10.1109/LGRS.2011.2174772.
- Kim, Y., van Zyl, J.J., 2009. A time-series approach to estimate soil moisture using polarimetric radar data. IEEE Trans. Geosci. Remote Sens. 47, 2519–2527. https:// doi.org/10.1109/TGRS.2009.2014944.
- Lagouarde, J.-P., Bach, M., Sobrino, J.A., Boulet, G., Briottet, X., Cherchali, S., Coudert, B., Dadou, I., Dedieu, G., Gamet, P., Hagolle, O., Jacob, F., Nerry, F., Olioso, A., Ottlé, C., Roujean, J., Fargant, G., 2013. The MISTIGRI thermal infrared project: scientific objectives and mission specifications. Int. J. Remote Sens. 34, 3437–3466. https://doi.org/10.1080/01431161.2012.716921.
- Laluet, P., Olivera-Guerra, L., Altés, V., Paolini, G., Ouaadi, N., Rivalland, V., Jarlan, L., Villar, J.M., Merlin, O., 2023. Retrieving the irrigation actually applied at district scale: assimilating high-resolution Sentinel-1-derived soil moisture data into a FAO-56-based model (preprint). Engineering. https://doi.org/10.31223/X54Q18.
- Le Toan, T., Ribbes, F., Wang, Li-Fang, Floury, N., Kung-Hau, Ding, Kong, Jin Au, Fujita, M., Kurosu, T., 1997. Rice crop mapping and monitoring using ERS-1 data based on experiment and modeling results. IEEE Trans. Geosci. Remote Sens. 35, 41–56. https://doi.org/10.1109/36.551933.
- Lee, J.-S., 1983. Digital image smoothing and the sigma filter. Comput. Vis. Graph. Image Process. 24, 255–269. https://doi.org/10.1016/0734-189X(83)90047-6.
- Lievens, H., Martens, B., Verhoest, N.E.C., Hahn, S., Reichle, R.H., Miralles, D.G., 2017. Assimilation of global radar backscatter and radiometer brightness temperature observations to improve soil moisture and land evaporation estimates. Remote Sens. Environ. 189, 194–210. https://doi.org/10.1016/j.rse.2016.11.022.
- Liu, C., Chen, Z., Shao, Y., Chen, J., Hasi, T., Pan, H., 2019. Research advances of SAR remote sensing for agriculture applications: a review. J. Integr. Agric. 18, 506–525. https://doi.org/10.1016/S2095-3119(18)62016-7.
- Liu, J., Pattey, E., Miller, J.R., McNairn, H., Smith, A., Hu, B., 2010. Estimating crop stresses, aboveground dry biomass and yield of corn using multi-temporal optical data combined with a radiation use efficiency model. Remote Sens. Environ. 114, 1167–1177. https://doi.org/10.1016/j.rse.2010.01.004.
- Liu, S., Peng, Y., Du, W., Le, Y., Li, L., 2015. Remote estimation of leaf and canopy water content in winter wheat with different vertical distribution of water-related properties. Remote Sens. 7, 4626–4650. https://doi.org/10.3390/rs70404626.
- properties. Remote Sens. 7, 4626–4650. https://doi.org/10.3390/rs/70404626. MacDonald, R.B., Hall, F.G., 1980. Global crop forecasting. Science 208, 670–679. https://doi.org/10.1126/science.208.4445.670.
- Maity, S., Patnaik, C., Chakraborty, M., Panigrahy, S., 2004. Analysis of temporal backscattering of cotton crops using a semiempirical model. IEEE Trans. Geosci. Remote Sens. 42, 577–587. https://doi.org/10.1109/TGRS.2003.821888.
- Mattia, F., Thuy Le Toan, Picard, G., Posa, F.I., D'Alessio, A., Notarnicola, C., Gatti, A.M., Rinaldi, M., Satalino, G., Pasquariello, G., 2003. Multitemporal c-band radar measurements on wheat fields. IEEE Trans. Geosci. Remote Sens. 41, 1551–1560. https://doi.org/10.1109/TGRS.2003.813531.
- $\label{lem:memory:mem$
- McNairn, H., Brisco, B., 2004. The application of C-band polarimetric SAR for agriculture: a review. Can. J. Remote Sens. 30, 525–542. https://doi.org/10.5589/ m03-069.
- McNairn, H., Jiao, X., Pacheco, A., Sinha, A., Tan, W., Li, Y., 2018. Estimating canola phenology using synthetic aperture radar. Remote Sens. Environ. 219, 196–205. https://doi.org/10.1016/j.rse.2018.10.012.
- McNairn, H., Kross, A., Lapen, D., Caves, R., Shang, J., 2014. Early season monitoring of corn and soybeans with TerraSAR-X and RADARSAT-2. Int. J. Appl. Earth Obs. Geoinf. 28, 252–259. https://doi.org/10.1016/j.jag.2013.12.015.
- McNairn, H., Shang, J., Jiao, X., Deschamps, B., 2012. Establishing crop productivity using RADARSAT-2. Int. Arch. Photogramm. Remote Sens. Spat. Inf. Sci. XXXIX-B8, 283–287. https://doi.org/10.5194/isprsarchives-XXXIX-B8-283-2012.
- Mercier, A., Betbeder, J., Baudry, J., Le Roux, V., Spicher, F., Lacoux, J., Roger, D., Hubert-Moy, L., 2020. Evaluation of Sentinel-1 & 2 time series for predicting wheat and rapeseed phenological stages. ISPRS J. Photogramm. Remote Sens. 163, 231–256. https://doi.org/10.1016/j.isprsjprs.2020.03.009.
- Montero, D., Aybar, C., Mahecha, M.D., Martinuzzi, F., Söchting, M., Wieneke, S., 2023. A standardized catalogue of spectral indices to advance the use of remote sensing in Earth system research. Sci. Data 10, 197. https://doi.org/10.1038/s41597-023-02006.0
- Ouaadi, N., Jarlan, L., Ezzahar, J., Zribi, M., Khabba, S., Bouras, E., Bousbih, S., Frison, P.-L., 2020. Monitoring of wheat crops using the backscattering coefficient and the interferometric coherence derived from Sentinel-1 in semi-arid areas. Remote Sens. Environ. 251, 112050 https://doi.org/10.1016/j.rse.2020.112050.
- Paloscia, S., Macelloni, G., Pampaloni, P., Sigismondi, S., 1999. The potential of C- and L-band SAR in estimating vegetation biomass: the ERS-1 and JERS-1 experiments. IEEE Trans. Geosci. Remote Sens. 37, 2107–2110. https://doi.org/10.1109/36.774723.

- Philip Robertson, G., Gross, K.L., Hamilton, S.K., Landis, D.A., Schmidt, T.M., Snapp, S.S., Swinton, S.M., 2014. Farming for ecosystem services: an ecological approach to production agriculture. BioScience 64, 404–415. https://doi.org/10.1093/biosci/ bin037
- Prevot, L., Champion, I., Guyot, G., 1993a. Estimating surface soil moisture and leaf area index of a wheat canopy using a dual-frequency (C and X bands) scatterometer. Remote Sens. Environ. 46, 331–339. https://doi.org/10.1016/0034-4257(93) 90053-7.
- Prevot, L., Dechambre, M., Taconet, O., Vidal-Madjar, D., Normand, M., Gallej, S., 1993b. Estimating the characteristics of vegetation canopies with airborne radar measurements. Int. J. Remote Sens. 14, 2803–2818. https://doi.org/10.1080/ 01431169308904310.
- Qadir, A., Skakun, S., Eun, J., Prashnani, M., Shumilo, L., 2023. Sentinel-1 time series data for sunflower (Helianthus annuus) phenology monitoring. Remote Sens. Environ. 295, 113689 https://doi.org/10.1016/j.rse.2023.113689.
- Rashid, A., 2003. Global information and early warning system on food and agriculture: appropriate technology and institutional development challenges. In: Zschau, J., Küppers, A. (Eds.), Early Warning Systems for Natural Disaster Reduction. Springer Berlin Heidelberg, Berlin, Heidelberg, pp. 337–344. https://doi.org/10.1007/978-3-642-55903-7 42.
- Robertson, P., Hamilton, S., 2015. Long-term ecological research in agricultural landscapes at the Kellogg Biological Station LTER site: conceptual and experimental framework. In: The Ecology of Agricultural Landscapes: Long-Term Research on the Path to Sustainability. Oxford University Press, New York, USA, pp. 1–32.
- Sanchez, A.H., Picoli, M.C.A., Camara, G., Andrade, P.R., Chaves, M.E.D., Lechler, S., Soares, A.R., Marujo, R.F.B., Simões, R.E.O., Ferreira, K.R., Queiroz, G.R., 2020. Comparison of cloud cover detection algorithms on sentinel–2 images of the amazon tropical forest. Remote Sens. 12, 1284. https://doi.org/10.3390/rs12081284.
- Skriver, H., Mattia, F., Satalino, G., Balenzano, A., Pauwels, V.R.N., Verhoest, N.E.C., Davidson, M., 2011. Crop classification using short-revisit multitemporal SAR data. IEEE J. Sel. Top. Appl. Earth Obs. Remote Sens. 4, 423–431. https://doi.org/ 10.1109/JSTARS.2011.2106198.
- Slafer, G.A., Savin, R., Sadras, V.O., 2023. Wheat yield is not causally related to the duration of the growing season. Eur. J. Agron. 148, 126885 https://doi.org/ 10.1016/j.eja.2023.126885.
- Steele-Dunne, S.C., Friesen, J., van de Giesen, N., 2012. Using diurnal variation in backscatter to detect vegetation water stress. IEEE Trans. Geosci. Remote Sens. 50, 2618–2629. https://doi.org/10.1109/TGRS.2012.2194156.
- Steele-Dunne, S.C., McNairn, H., Monsivais-Huertero, A., Judge, J., Liu, P.-W., Papathanassiou, K., 2017. Radar remote sensing of agricultural canopies: a review. IEEE J. Sel. Top. Appl. Earth Obs. Remote Sens. 10, 2249–2273. https://doi.org/ 10.1109/JSTARS.2016.2639043.
- Suyker, A.E., Verma, S.B., Burba, G.G., Arkebauer, T.J., 2005. Gross primary production and ecosystem respiration of irrigated maize and irrigated soybean during a growing season. Agric. For. Meteorol. 131, 180–190. https://doi.org/10.1016/j. agrformet.2005.05.007.
- Tao, L., Li, J., Jiang, J., Chen, X., 2016. Leaf area index inversion of winter wheat using modified water-cloud model. IEEE Geosci. Remote Sens. Lett. 13, 816–820. https:// doi.org/10.1109/LGRS.2016.2546945.
- Torres, R., Snoeij, P., Geudtner, D., Bibby, D., Davidson, M., Attema, E., Potin, P., Rommen, B., Floury, N., Brown, M., Traver, I.N., Deghaye, P., Duesmann, B., Rosich, B., Miranda, N., Bruno, C., L'Abbate, M., Croci, R., Pietropaolo, A., Huchler, M., Rostan, F., 2012. GMES Sentinel-1 mission. Remote Sens. Environ. 120, 9–24. https://doi.org/10.1016/j.rse.2011.05.028.
- Tucker, C.J., 1979. Red and photographic infrared linear combinations for monitoring vegetation. Remote Sens. Environ. 8, 127–150. https://doi.org/10.1016/0034-4257 (79)90013-0.

- Tucker, C.J., Vanpraet, C.L., Sharman, M.J., Van Ittersum, G., 1985. Satellite remote sensing of total herbaceous biomass production in the senegalese sahel: 1980–1984. Remote Sens. Environ. 17, 233–249. https://doi.org/10.1016/0034-4257(85)
- Ulaby, F.T., Allen, C.T., Eger, G., Kanemasu, E., 1984. Relating the microwave backscattering coefficient to leaf area index. Remote Sens. Environ. 14, 113–133. https://doi.org/10.1016/0034-4257(84)90010-5.
- Ulaby, F.T., Moore, R.K., Fung, A.K., 1981. Microwave Remote Sensing. 1: Microwave Remote Sensing, Fundamentals and Radiometry. Artech House, Norwood, Mass.
- Ulaby, F., Wilson, E., 1985. Microwave attenuation properties of vegetation canopies. IEEE Trans. Geosci. Remote Sens. GE 23, 746–753. https://doi.org/10.1109/
- Van Der Velde, M., Van Diepen, C.A., Baruth, B., 2019. The European crop monitoring and yield forecasting system: celebrating 25 years of JRC MARS bulletins. Agric. Syst. 168, 56–57. https://doi.org/10.1016/j.agsy.2018.10.003.
- Veloso, A., Mermoz, S., Bouvet, A., Le Toan, T., Planells, M., Dejoux, J.-F., Ceschia, E., 2017. Understanding the temporal behavior of crops using Sentinel-1 and Sentinel-2like data for agricultural applications. Remote Sens. Environ. 199, 415–426. https:// doi.org/10.1016/j.rse.2017.07.015.
- Verma, S.B., Dobermann, A., Cassman, K.G., Walters, D.T., Knops, J.M., Arkebauer, T.J., Suyker, A.E., Burba, G.G., Amos, B., Yang, H., Ginting, D., Hubbard, K.G., Gitelson, A.A., Walter-Shea, E.A., 2005. Annual carbon dioxide exchange in irrigated and rainfed maize-based agroecosystems. Agric. For. Meteorol. 131, 77–96. https:// doi.org/10.1016/j.agrformet.2005.05.003.
- Vermunt, P.C., Steele-Dunne, S.C., Khabbazan, S., Kumar, V., Judge, J., 2022. Towards understanding the influence of vertical water distribution on radar backscatter from vegetation using a multi-layer water cloud model. Remote Sens 14, 3867. https:// doi.org/10.3390/rs14163867.
- Vreugdenhil, M., Navacchi, C., Bauer-Marschallinger, B., Hahn, S., Steele-Dunne, S., Pfeil, I., Dorigo, W., Wagner, W., 2020. Sentinel-1cross ratio and vegetation optical depth: a comparison over Europe. Remote Sens 12, 3404. https://doi.org/10.3390/rs12203404.
- Vreugdenhil, M., Wagner, W., Bauer-Marschallinger, B., Pfeil, I., Teubner, I., Rüdiger, C., Strauss, P., 2018. Sensitivity of sentinel-1 backscatter to vegetation dynamics: an austrian case study. Remote Sens. 10, 1396. https://doi.org/10.3390/rs10091396.
- Whitcraft, A., Becker-Řeshef, I., Justice, C., 2015a. A framework for defining spatially explicit earth observation requirements for a global agricultural monitoring initiative (GEOGLAM). Remote Sens 7, 1461–1481. https://doi.org/10.3390/rs70201461
- Whitcraft, A.K., Vermote, E.F., Becker-Reshef, I., Justice, C.O., 2015b. Cloud cover throughout the agricultural growing season: Impacts on passive optical earth observations. Remote Sens. Environ. 156, 438–447. https://doi.org/10.1016/j. rse.2014.10.009.
- Wiegand, C., Richardson, A., Jackson, R., Pinter, P., Aase, J., Smika, D., Lautenschlager, L., McMurtrey, J., 1986. Development of agrometeorological crop model inputs from remotely sensed information. IEEE Trans. Geosci. Remote Sens. GE 24, 90–98. https://doi.org/10.1109/TGRS.1986.289689.
- Wiseman, G., McNairn, H., Homayouni, S., Shang, J., 2014. RADARSAT-2 Polarimetric SAR response to crop biomass for agricultural production monitoring. IEEE J. Sel. Top. Appl. Earth Obs. Remote Sens. 7, 4461–4471. https://doi.org/10.1109/ JSTARS.2014.2322311.
- Zhang, X., Zhang, Q., 2016. Monitoring interannual variation in global crop yield using long-term AVHRR and MODIS observations. ISPRS J. Photogramm. Remote Sens. 114, 191–205. https://doi.org/10.1016/j.isprsjprs.2016.02.010.
- Zhu, Z., Wang, S., Woodcock, C.E., 2015. Improvement and expansion of the Fmask algorithm: cloud, cloud shadow, and snow detection for Landsats 4–7, 8, and Sentinel 2 images. Remote Sens. Environ. 159, 269–277. https://doi.org/10.1016/j. rse.2014.12.014.